School of Electronic Engineering
and Computer Science

APRIL 23, 2019

FINAL REPORT

MEng Computer Systems Engineering

IMAGE RECONSTRUCTION FROM MULTIPLE OCT PARTIAL IMAGES

FINAL YEAR UNDERGRADUATE PROJECT 2018/2019

ASTRID FLORIO

SUPERVISORS: DR ROBERT DONNAN, DR PETER TOMLINS

ABSTRACT

Optical coherence tomography (OCT) is an optical imaging method. It can be considered analogous to ultrasound imaging with greater resolution but lower penetration depth. OCT cannot penetrate the tooth fully to observe tooth decay in-between teeth, since this area cannot be accessed directly, unlike with X-rays.

This project attempts to reconstruct a 3D image of a tooth from partial 2D images taken from the side of a tooth which are normally accessible. Various techniques were explored both in terms of image capture and image registration.

ACKNOWLEDGEMENTS

I would like to thank Dr Donnan and Dr Tomlins (SMD) for the help in this project and my student advisor Dr Phillips for the help throughout my course.

TABLE OF CONTENTS

INDEX

Abbreviations

CCD: charge-coupled device
IR: infra-red (light)
FD-OCT: frequency-domain OCT
OCT: optical coherence tomography
SLD: super luminescent diode
SD-OCT: spectral-domain OCT
SS-OCT: swept-source OCT
TD-OCT: time-domain OCT

Figures

Tables

Code snippets

Equations

1 INTRODUCTION

Medical imaging has been a part of dentistry for over a century now. In fact, it was only a few weeks after the accidental discovery of X-Rays by Konrad Wilhelm von Roentgen, that the first dental X-Ray image was taken by German dentist Otto Walkhoff. (Castellucci, 2005)

Since then, 2-D radiographs have provided "excellent images for most dental radiographic needs" (Shah, 2014). However, "a significant constraint of conventional radiography is the superimposition of overlying structures, which obscures the object of interest" (Shah, 2014).

Another issue in dental imaging is the radiation dose: it wasn't long after the discovery of X-Rays that the effect of exposure to ionizing radiation became apparent. (Castellucci, 2005) Even to this day, despite the progress that has been made in the field of medical imaging, radiation exposure remains a risk to both patients and medical professionals.

According to the FDA the risk to develop cancer from X-Ray exposure depends on radiation dose, patient's age (the risk being greater on younger patients), patient's sex (women having a "somewhat higher" risk than men) and body region. (U.S. Food and Drug Administration, 2018).

Table 1 Comparison of 2D and 3D imaging techniques (Erten & Yimlaz, 2018)

IMAGING TECHNIQUES	EFFECTIVE DOSE (µSV)	COST
Periapical radiograph	<1.5	X
Panoramic radiograph	2.7-24.3	2X
Cephalometric radiograph	<6	2X
CBCT		
Dentoalveolar CBCT	11-674(61)	
Maxillofacial CBCT	30-1073	10-20X
MSCT maxillo-mandibular	280-1410	10-20X

Thanks to the introduction of 3D imaging techniques, "it was possible to evaluate structures in real three anatomical dimensions" (Erten & Yimlaz, 2018) with the added benefit that most of these are non-invasive techniques, thus not involving ionizing radiation. However the high cost of these techniques remains a significant barrier to orthodontic use.

Table 2 Comparison of cost, radiation dose and indications of 3D imaging techniques (Erten & Yimlaz, 2018)

IMAGING TECHNIQUE	COST	RADIATION DOSE	INDICATIONS
CBCT	High	Dentoalveolar 11-674 µSv	Craniofacial deformities (other indications with caution)
		Maxillofacial 30-1073 µSv	

Laser scanner	High	Non-invasive	May be recommended in every patient
Stereo photogrammetry	High	Non-invasive	May be recommended in every patient
MRI	High	Non-invasive	Airway assessment
Intraoral scanner	High	Non-invasive	May be recommended in every patient

1.1 Motivation

Optical coherence tomography is a cost-effective imaging technique that employs near-infrared light to produce high definition 2D and 3D images. However, like other techniques employing long wavelength light, it cannot penetrate the tooth fully and therefore can only image the surface.

Because tooth decay can form in-between teeth, OCT is generally considered unsuitable if the area cannot be accessed directly.

1.2 Aims and Objectives

The aim of this project is to investigate if and to what extent it is possible to use partial OCT images to reconstruct a full 3D image of a tooth including the areas which cannot be directly imaged.

To test this, the objective is to utilize a rotating stage, to take images of sections of teeth at different angles, settings and note how well a reconstruction can be performed.

1.2.1 **Project requirements**

- Implement a rotating stage on present OCT instrument
- Develop a MATLAB code to allow reconstruction of 3D images from a sequence of 2D scans at varying angles.

2 BACKGROUND

2.1 Key Concepts

2.1.1 **Coherence**

Coherency is a property of light. A light source is said to be coherent when all the photons in it have the same frequency and constant or zero phase difference.

A light beam which is only coherent over a short distance, generally in the order of tens of microns (Popescu, n.d.), is defined as a low-coherence light source.

A coherent light source is necessary to form stable interference patterns (Encyclopædia Britannica, Inc., n.d.).

2.1.2 **Reflection**

"Reflection, abrupt change in the direction of propagation of a wave that strikes the boundary between different mediums" (Encyclopaedia Britannica, Inc., n.d.).

The angle of reflection is a function of the angle of incidence. In the case of a perfectly reflective surface, the angle of incidence is equal to the angle of reflection.

$$\theta_i = \theta_r$$

Equation 1 Perfectly reflective surface

Reflection at rough, or irregular, boundaries is diffuse. The reflectivity of a surface material is the fraction of energy of the oncoming wave that is reflected by it" (Encyclopaedia Britannica, Inc., n.d.).

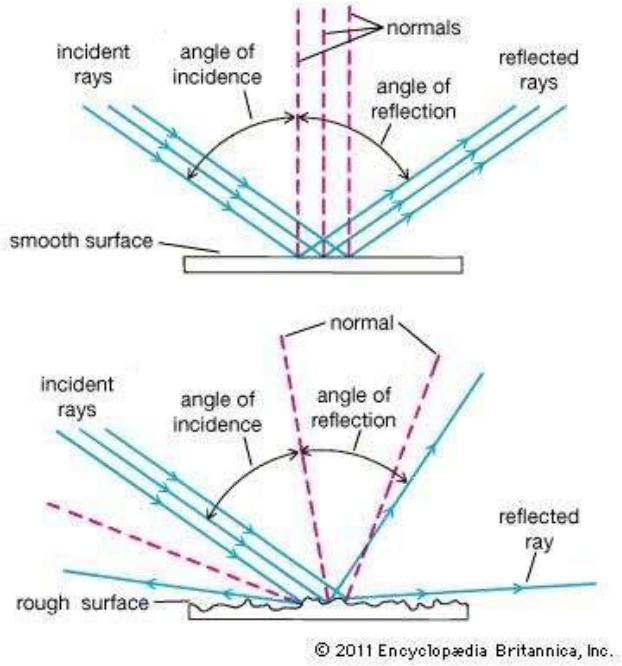

Figure 1 Reflection on a homogenous vs inhomogeneous surface (Encyclopaedia Britannica, Inc., n.d.)

2.1.3 **Refraction**

"Refraction, in physics, the change in direction of a wave passing from one medium to another caused by its change in speed" (Encyclopædia Britannica, Inc., n.d.).

The relationship between angles of incidence and refraction is defined by **Snell's Law**:

Equation 2 Snell's Law

$$\frac{sin\theta_2}{\sin\theta_1} = \frac{v_2}{v_1} = \frac{n_1}{n_2}$$

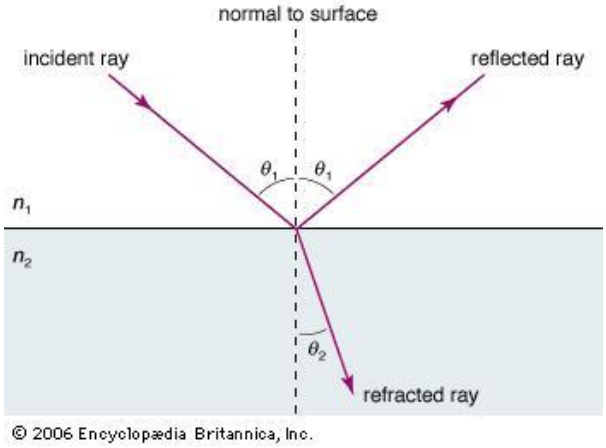

Figure 2 Refraction (Encyclopaedia Britannica, Inc., n.d.)

If light in a transparent medium approaches a boundary with another transparent medium with lower refractive index, at an angle greater than what is known as **critical angle**, the light will be completely reflected within the medium. This is called **total internal reflection**.

Equation 3 The critical angle is defined as the incidence angle which results in a 90-degrees refraction angle

$$n_i \cdot \sin\theta_{crit} = n_r \cdot \sin\theta_r$$

$$n_i \cdot \sin\theta_{crit} = n_r \cdot \sin 90°$$

$$since\ \sin 90° = 1 \implies \sin\theta_{crit} = \frac{n_r}{n_i}$$

$$\therefore \theta_{crit} = \sin^{-1}\left(\frac{n_r}{n_i}\right)$$

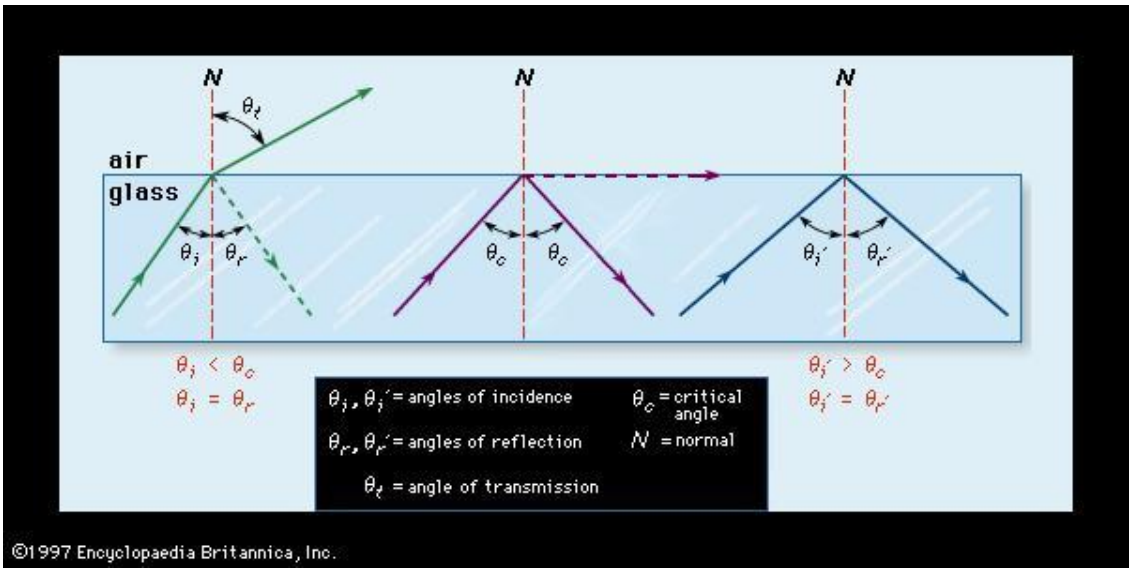

Figure 3 Total internal reflection (Encyclopaedia Britannica, Inc., n.d.)

If the incidence angle is lower than the critical angle, part of the beam will be reflected, and part refracted.

2.1.4 **Optical Heterodyne Detection**

Optical Heterodyne Detection is a detection method also known as **coherent detection**, where "a weak input signal is mixed with a local oscillator wave in a nonlinear device such as a rectifier, and the resulting mixing product is then detected, often after filtering out the original signal and the local oscillator frequency. "The frequency of the mixing product is the sum or the difference of the frequencies of the signal and the local oscillator" (Paschotta, n.d.).

Optical Heterodyne Detection involves a photodiode, a local oscillator and a beam-splitter (or a fibre-coupler in a fibre-optic setup). The output is an electrical signal.

"The mixing product is not obtained by mixing the signal and local oscillator wave in a nonlinear crystal, but rather simply by detecting the linearly superimposed waves with a square-law photodetector, typically a photodiode" (Paschotta, n.d.).

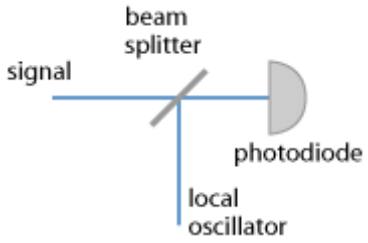

Figure 4 Optical Heterodyne Detection (Paschotta, n.d.)

2.1.5 **Michelson Interferometer**

The Michelson Interferometer is a configuration for optical interferometry which produces an interference pattern by splitting a monochromatic light beam in two arms.

One beam is directed towards a fixed mirror and another towards a movable mirror. Both beams are reflected into the beam-splitter, resulting in an interference pattern (Georgia State University, n.d.).

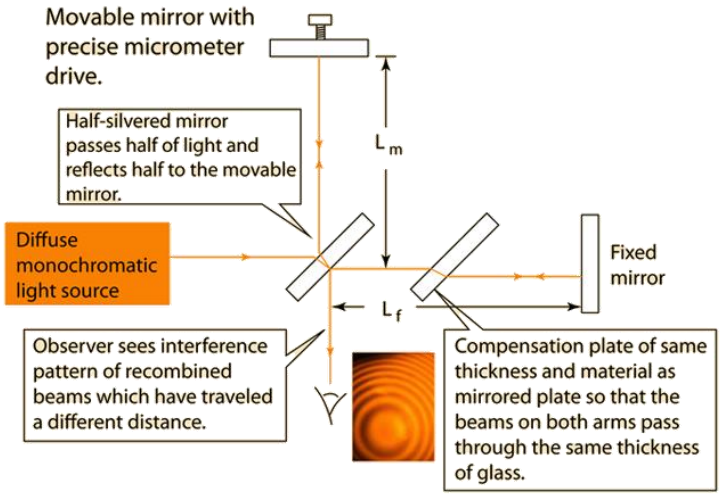

Figure 5 Michelson Interferometer (Georgia State University, n.d.)

2.2 Dentistry Terminology

Some terminology commonly used in dentistry is used in this report:

BUCCAL	"relating to, near, involving, or supplying a cheek" (Merriam-Webster, n.d.)
LINGUAL	"relating to or being the surface of a tooth next to the tongue" (Merriam-Webster, n.d.)
OCCLUSAL	"relating to the grinding or biting surface of a tooth" (Merriam-Webster, Incorporated, n.d.)
PROXIMAL	"the mesial and distal surfaces of a tooth" (Merriam-Webster, n.d.)

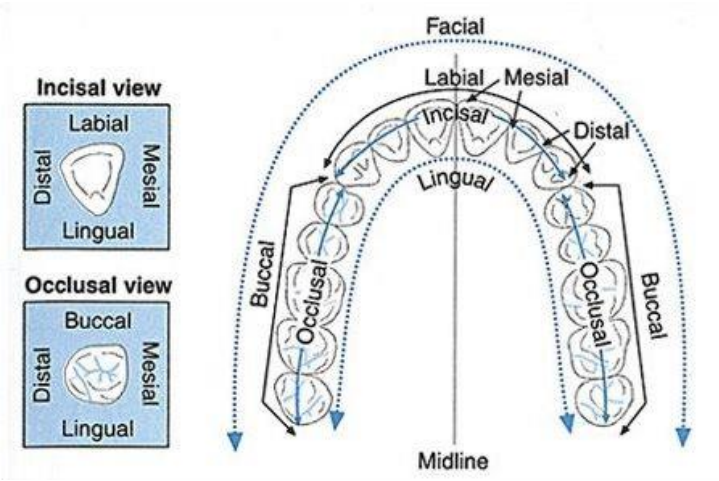

Figure 6 Terminology relating to teeth (Ballantyne Endodontics, 2018)

2.3 Dental Imaging Techniques

2.3.1 **X-Ray**

An X-Ray image, also known as roentgenogram, is obtained by shining X-Rays through a sample to produce a shadow on an X-ray sensitive film.

Because x-rays are completely penetrative (meaning they can "see completely through"), they are one of the preferred methods of dental imaging.

The main drawback to x-ray imaging is that diagnostic X-rays pose a risk to the health of both patients and doctors as they increase the risk of developing cancers. They also pose an increased risk to unborn babies and can potentially lead to miscarriage in pregnant women.

2.3.1.1 X-Ray micro tomography

X-Ray micro tomography, also called X-Ray micro-CT (computerized tomography) is a high resolution, non-destructive 3D imaging technique which uses X-Rays to capture images with a resolution in the range of hundreds of nanometres to centimetres (NASA, n.d.).

2.3.2 **Transillumination**

Transillumination consists in shining light through tissues to highlight features such as cavities, infections or enamel damage.

2.3.2.1 DIAGNOcam

The DIAGNOcam is an intraoral imaging device produced by KaVo Dental, which consists of an **infra-red (IR) light** source and camera, which uses the principle of transillumination to capture images and videos of teeth.

"The tooth becomes a light conductor, making the tooth structures visible: Any areas with caries or cracks that the light comes across on its way to the tooth surface are clearly demarcated and visibly darker" (KaVo Dental, n.d.).

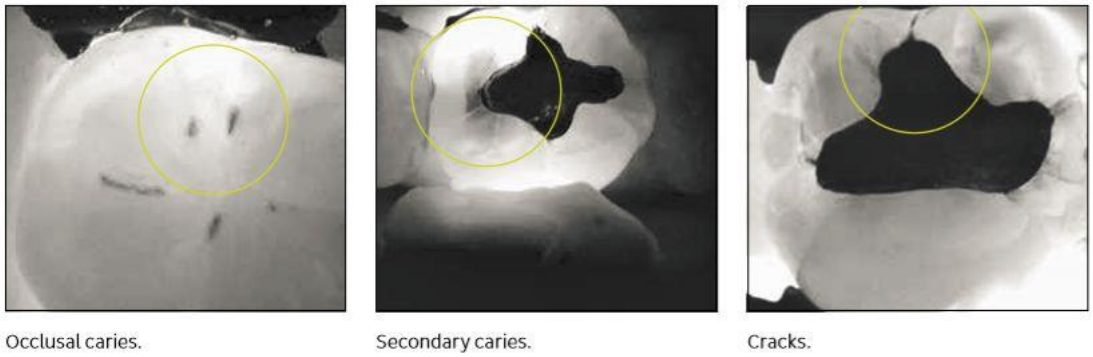

Figure 7 DIAGNOcam images (KaVo Dental, n.d.)

The major advantages of this instrument are that it can provide immediate high-quality images as well as highlighting damage and cavities without exposing the patient to ionizing radiation (as is the case with X-rays). One major drawback, however, is that IR light is not fully penetrative and cannot provide images of deep structures (as for example a root).

2.4 Optical Coherence Tomography

Optical coherence tomography (OCT) is an optical imaging method which allows non-invasive, high resolution cross-sectional three-dimensional imaging of samples within an axial resolution of 5 µm or less (ThorLabs, Inc., n.d.).

OCT can be considered analogous to ultrasound imaging, with a resolution "one to two orders of magnitude finer than the ones achieved through conventional ultrasound" (Popescu, et al., 2011), albeit with an imaging depth limited to a few millimetres (Optical and Biomedical Engineering Laboratory, University of Western Australia, n.d.).

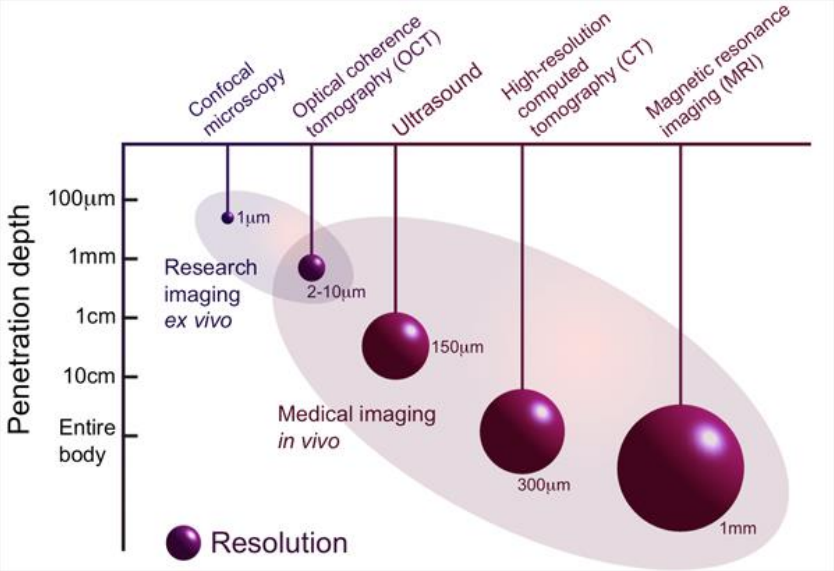

Figure 8: Comparison of the resolution and penetration depth of various imaging methods (Optical and Biomedical Engineering Laboratory, University of Western Australia, n.d.).

2.4.1 **Time-Domain OCT**

OCT uses low-coherence interferometry, usually in a fibre-based Michelson setup (Figure 9). (ThorLabs, Inc., n.d.)

"In low-coherence reflectometry, the coherence property of light reflected from a sample provides information on the time-of-flight delay from the reflective boundaries and backscattering sites in the sample." (Huang, et al., 1991)

The setup is a fibre optic Michelson interferometer, where a **super luminescent diode (SLD)** is used to provide a low coherence light source.

The light from the source is split by the coupler and directed towards both the interferometer arm (where the sample is placed) and the reference arm. In the reference arm the light is backscattered by a reference mirror and propagates back. In the sample arm the light is backscattered by the sample (Popescu, et al., 2011).

"The returning light from both arms recombine at the coupler and generate an interference pattern" (Popescu, et al., 2011). Since "the interferometric signal is modulated at a high frequency by Doppler shift and piezoelectric modulation" (Huang, et al., 1991), the output is frequency-filtered to separate the signal from the noise (Huang, et al., 1991).

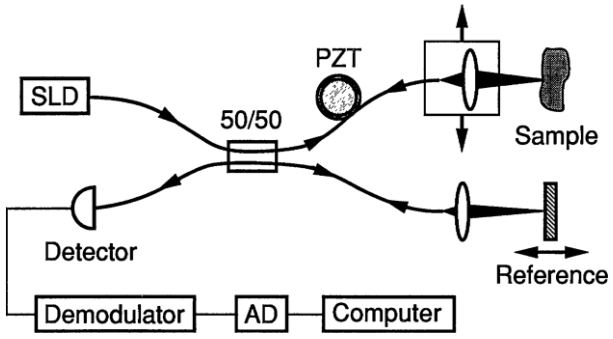

Figure 9: An OCT system in a Michelson setup (Huang, et al., 1991)

The reference mirror is moved longitudinally, thus creating an interference pattern only with light reflected from an equivalent distance to the light within the sample (Popescu, et al., 2011). At the same time the optical beam in the sample arm is moved laterally (Huang, et al., 1991).

"The OCT signal recorded by the detector during a complete travel of the reference mirror is called a depth scan or an **A-scan**" (Popescu, et al., 2011). A set of consecutive A-scans where the sample beam is moved across the sample is necessary to form a 2D OCT image (also referred to as **B-scan**).

This approach is known as **time-domain (TD)-OCT** because time delay information is used (Gabriele, et al., 2011).

2.4.2 Frequency-Domain OCT

Implementing a broad-bandwidth light source improved axial resolution from about 10µ to as low as 2 µm (Gabriele, et al., 2011). This is known as **frequency-domain (FD)-OCT**.

"Acquisition speed has improved considerably by detecting backscattering signals in the frequency domain" (Gabriele, et al., 2011), allowing depth information to be recorded without needing to move the reference mirror.

Because acquisition speed is reduced, artefacts due to sample movement are rarer than in TD-OCT. FD-OCT also has a higher signal-to-noise ratio which results in higher detection sensitivity.

"With these speed and sensitivity improvements, it is now feasible to collect volumetric (three-dimensional; 3D) scans of tissue, whereas in the past, the amount of time required to do this would have been prohibitive" (Gabriele, et al., 2011).

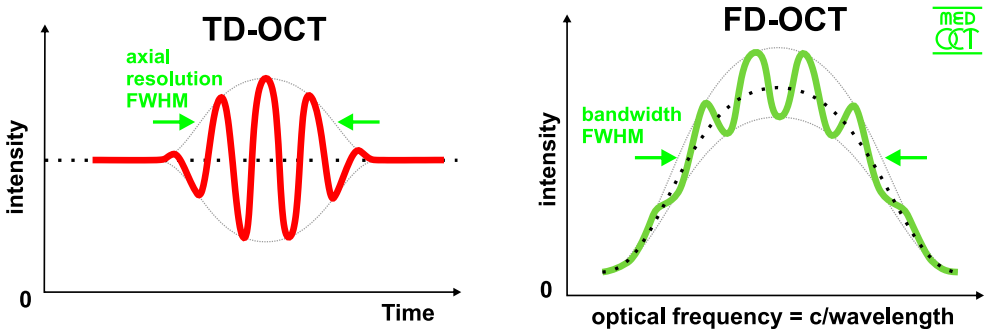

Figure 10 Interference TD-OCT vs FD-OCT (wikimedia.org, n.d.)

2.4.2.1 Spectral Domain OCT

In **spectral Domain (SD)-OCT**, frequency information is collected using a charge-coupled device (CCD) camera and a spectrometer.

One significant drawback of SD-OCT is a "noticeable drop-off in signal with depth" (Gabriele, et al., 2011). This is caused by the finite pixel size of the CCD camera but can be reduced by reducing the pixel size of the CCD camera (Gabriele, et al., 2011).

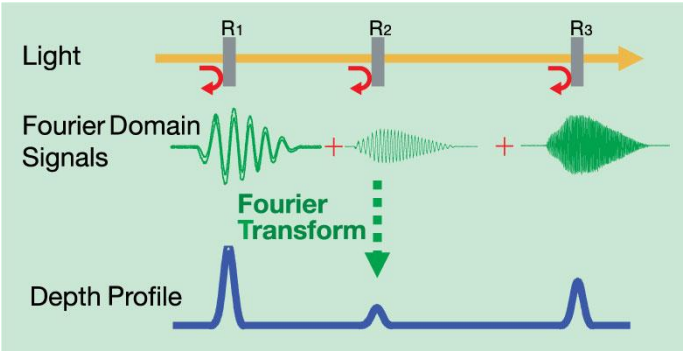

Figure 11 SD-OCT (ThorLabs, Inc., n.d.)

2.4.2.2 Swept Source OCT

Swept-source (SS)-OCT "obtains time-encoded spectral information by sweeping a narrow-bandwidth laser through a broad optical spectrum" (Gabriele, et al., 2011), contrary to SD-OCT.

A photodetector is used to detect backscattered light.

The main advantage of SS-OCT is that SS-OCT can be achieved with a simple photoreceptor, in contrast to SD-OCT which requires a CCD camera and a spectrometer. Additionally, the signal drop-off which occurs in SD-OCT with depth doesn't affect SS-OCT because of the narrow bandwidth (Gabriele, et al., 2011).

Table 3 Comparison of OCT techniques[1]

	Light Source	Primary Advantages	Primary Disadvantages
TD-OCT	Broad-bandwidth	Intensity information acquired in time domain; no complex conjugate image	Moving reference mirror required limiting acquisition rate
SD-OCT	Broad-bandwidth	No moving reference mirror required; higher sensitivity than TD-OCT. High scanning speed and axial resolution have been attained	Noticeable signal drop-off with depth
SS-OCT	Narrowband, swept through broad range	No moving reference mirror required; Higher sensitivity than TD-OCT; Very high scanning speeds can be attained; minimal signal drop-off with depth	Most ophthalmic systems operating at longer wave lengths (λ = 1-1.3 μm), with lower axial resolution

[1] Adapted from Gabriele et al. (Gabriele, et al., 2011)

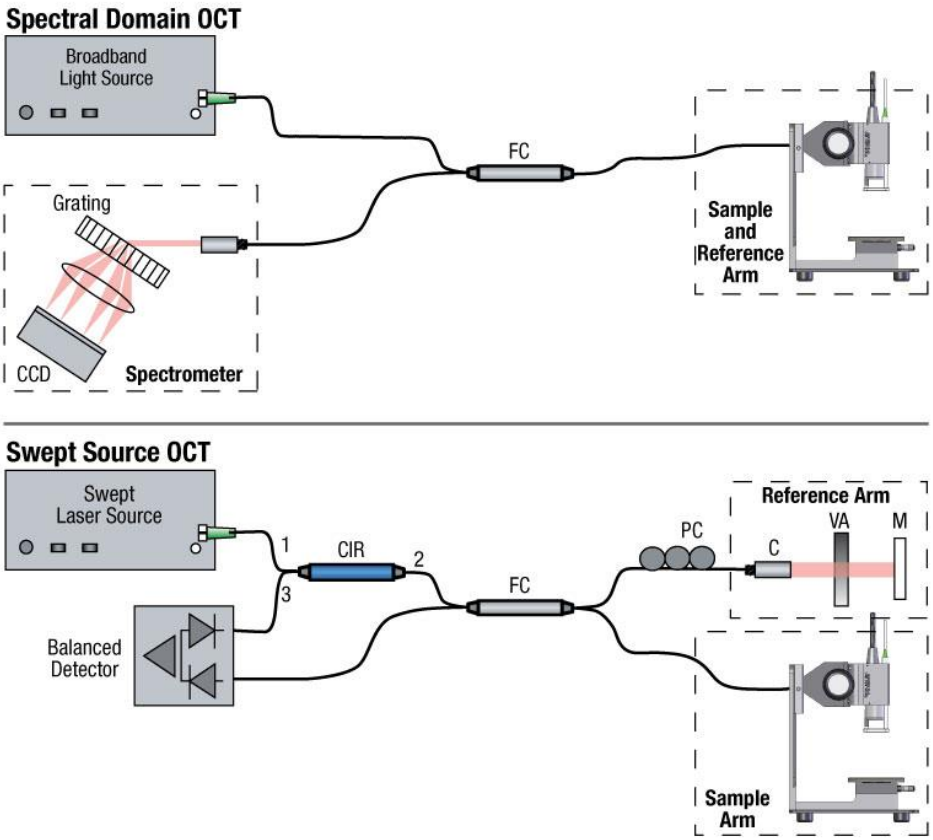

Figure 12 Comparison of SD-OCT and SS-OCT setups (ThorLabs, Inc., n.d.)

2.4.3 **Advantages & Limitations**

Compared to other imaging techniques such as X-Rays or Magnetic Resonance Imaging, OCT requires low amounts of computation to reconstruct the image (Huang, et al., 1991).

There are, however, some limitations due to reflecting structures in biological samples.

For example, “the presence of speckle noise will prevent the detection of subtle differences in tissue backscattering properties. In turbid media such as the vascular wall, multiply scattered light (echoes) retains enough coherence to be detected by the OCT system. These echoes will limit the depth range of OCT in situations where scattering predominates over absorption” (Huang, et al., 1991).

2.5 MATLAB

MATLAB is a high-performance language and integrated desktop environment (IDE) targeted at technical computation and iterative analysis.

MATLAB also includes an extensive collection of libraries (some user-generated) for a variety of applications.

The MATLAB Integrated Development Environment (IDE) also provides resources to automatically convert MATLAB code to other languages such as C, C++ and HDL, allowing to

rapidly deploy MATLAB code on an embedded processor or field programmable gate array (FPGA) or application-specific integrated circuit (ASIC).

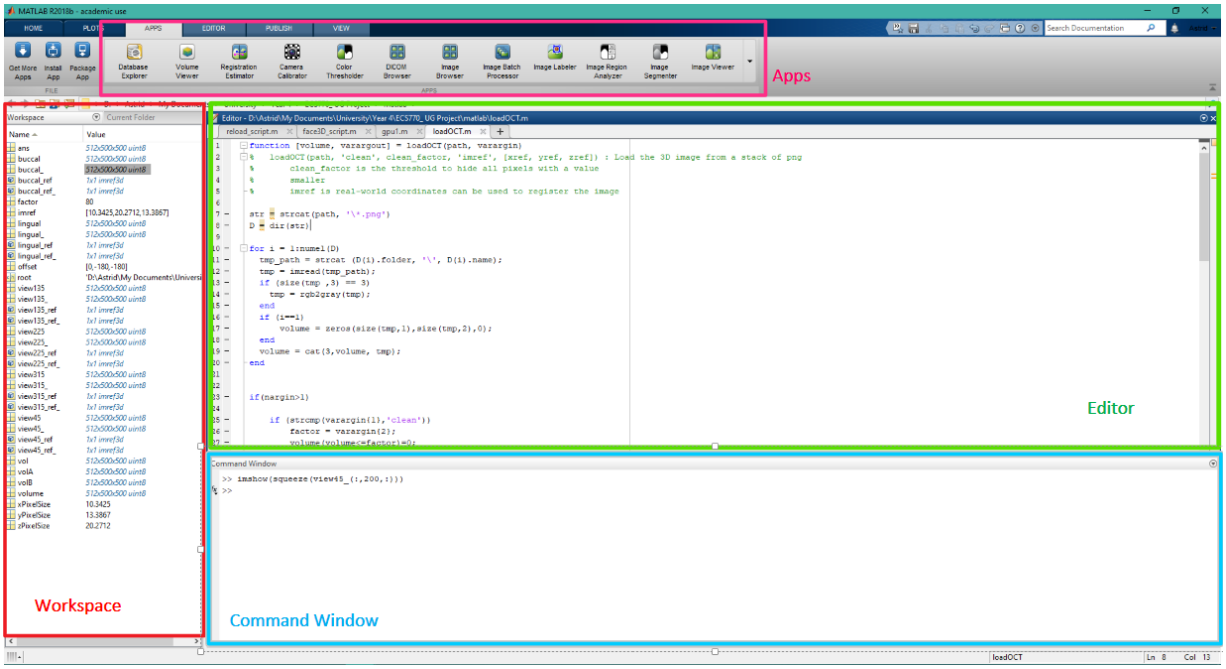

Figure 13 The MATLAB IDE

The MATLAB IDE is divided into an *editor*, a *command window*, and a *workspace*. The editor allows to edit and run scripts and functions; likewise, it is possible to run functions using the command window.

The workspace contains all variable created by the "main" script being run (although it is possible to examine variables inside a function using the workspace if the program is paused or has a breakpoint. The variable in the workspace are not deleted after the script runs and remain until the IDE is closed unless explicitly cleared. This allows to use the variables in a new script or in the command line, or even while the execution of a script is paused.

The MATLAB engine uses a Just-In-Time (JIT) compiler which generate native machine language code when the code is run and without having to explicitly compile it. (Shure, 2016)

2.5.1 **Image processing using MATLAB**

To process the image the Image Processing Toolbox was used (MathWorks, 2019).

"MATLAB stores most images as two-dimensional matrices, in which each element of the matrix corresponds to a single discrete *pixel* in the displayed image." (MathWorks, n.d.) For example a 3D image of 500 x 500 x 500 pixels is stored as 500 500x500 pixels images (also referred to as *image stack*). The image would be read into a matrix (also referred to as a *volume*), in the current workspace. This is not a permanent object and it needs to be reloaded from the *image stack*.

2.5.2 **Vectorization**

One of the most important features of the MATLAB language is that it is designed for operations involving matrices and vectors[2]. This means that, for example, performing an operation on every element in a vector does not require the use of a loop.

This does not only reflect a different syntax, but also compiler-level optimization of element-wise operations.

This means it is possible to achieve significant improvement by doing what is known as *vectorization*, that is *"the process of revising loop-based, scalar-oriented code to use MATLAB matrix and vector operations"* (MathWorks, n.d.).

As an example, the code below (Snippet 1)is part of the function used to import images stacks into the workspace; modifying the code from using loop statements to using vectorization reduced the execution time by almost 10 times (Table 4).

Snippet 1 Code using loop-structure (left) vs code using vectorization (right)

```
for i = 4:size(volume,1)
    for j = 4:size(volume,2)
        for z = 4:size(volume,3)
            tmp = volume(i,j,z);
            if (tmp < factor)
                volume(i,j,z) = 0;
            end
        end
    end
end
```

```
volume(volume<=factor)=0;
```

Table 4 Execution time of loop structure vs vectorization

FUNCTION	SELF-TIME
Function using loop structure (left)	3.4s
Function using vectorisation (right)	37.9s

2.6 Image registration methods review

Image registration is the process to align a pair of images. Image registration algorithms can be broadly divided into two groups: *direct methods*, and *feature-based methods*. (Szeliski, 2006)

2.6.1 **Direct methods**

Direct methods approach uses pixel-to-pixel matching to align images.

[2] In fact, the name MATLAB stands for "matrix laboratory" (Cooperative Institute for Meteorological Satellite Studies Space Science and Engineering Center (SSEC), University of Wisconsin-Madison, n.d.).

The process can be broken in two: first an *error metric* is chosen to compare the images, then an *optimization function* is used to find a minimum with respect to the error metric adopted.

Mean square error is a common error metric which looks "element-wise difference between two input images" (MathWorks, 2019). Other metrics can be used to account for the nature of the images to be registered: for example techniques applying *spatially varying weights* to each pixel (e.g. a metric function biased in favour of parts of the images that overlap in a case where the area where the images overlap is small). (Szeliski, 2006)

Optimization techniques also vary from simple (e.g. a *gradient descent algorithm*) to more complex ones such as *hierarchical motion estimation* which build a pyramid representation of the image (that is "the target is convolved with copies of the image reduced in scale" (Adelson, et al., 1984)) to perform the optimization search over a smaller number of pixels.

2.6.2 **Feature-based methods**

The feature-based approach to image registration involves extracting distinctive features to be matched between the images to estimate the geometric transformation. This approach can also be broken in two parts: first the features to be matched must be identified either manually (what is known as *control points selection*) or by means of a machine learning/computer vision method; secondly, after the matching features have been identified, an optimization function is used to estimate the geometric transformation required. (Szeliski, 2006)

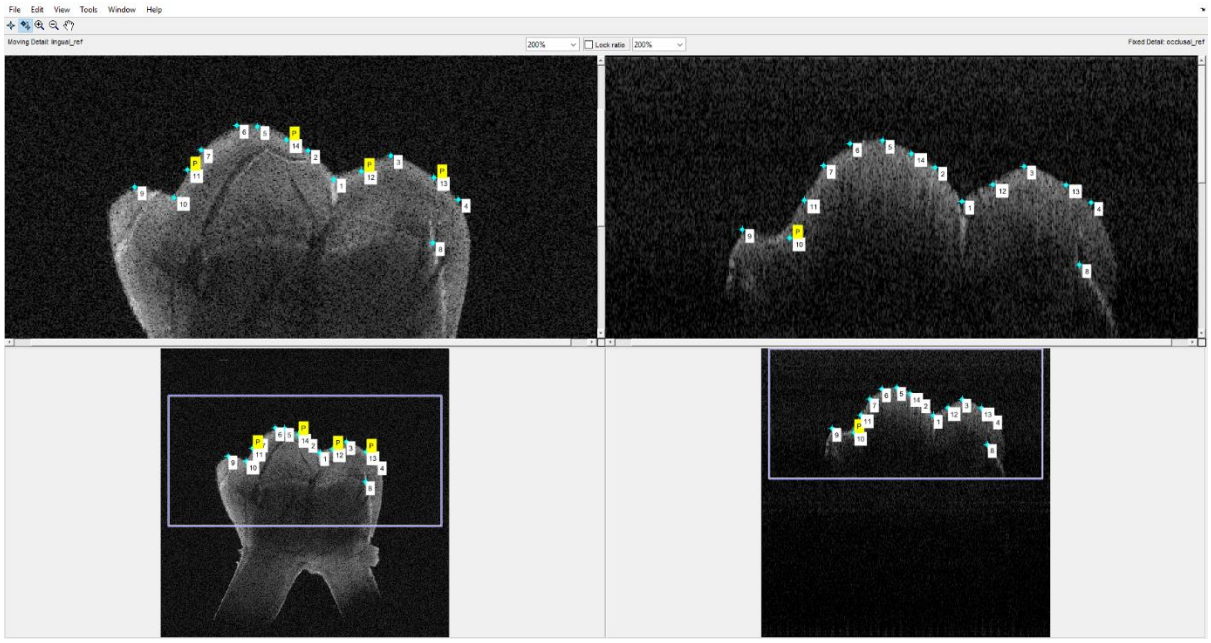

Figure 14 Control point feature in MATLAB

3 METHODOLOGY

3.1 Project Aims

Of the original stated aims as per the Project Specification:

1) Modification of OCT instrument with rotation stage
2) Imaging using modified OCT instrument
3) 3D composite image reconstruction
4) Image reconstruction optimization

The modification of the rotating stage was already completed by the time the work started. The focus was then shifted towards image reconstruction optimization using image registration techniques to increase the accuracy of the obtained 3D images.

3.2 Image sampling

To capture the images a rotating stage was mounted on the SD-OCT scanner in the Whitechapel Dentistry Hospital lab. This was used to capture images of a tooth at different angles.

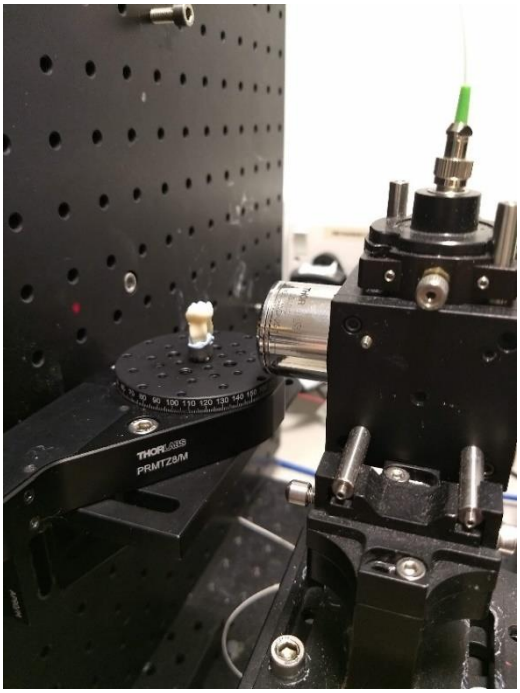

Figure 15 Rotating stage with tooth

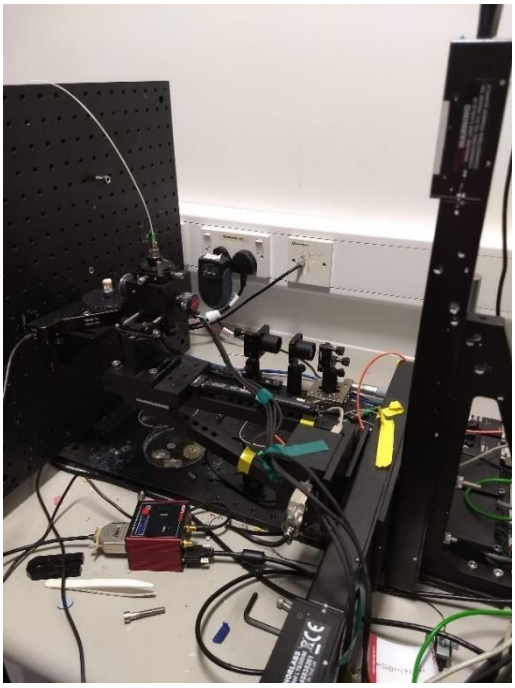

Figure 16 SD-OCT scanner

The stage and the arm of the OCT scanner were controlled by a computer using *OCTview-Lab ,* an OCT control software developed in-house at Queen Mary University of London (OCT lab at Queen Mary University of London, 2016).

This setup was used to capture two types of images[3]:

1. A “theta-stack” i.e. 360° image of a tooth consisting of a single B-scan taken at every degree interval rotating the tooth around its height (x-axis) (Figure 17)
2. A “y-stack”, i.e. a “flat” image at a fixed angle with multiple B-scans taken along the width of the tooth (y-axis) (Figure 18)

[3] All the images were captured at 1000kHz

These images, along with some previously captured by Dr Tomlins were used to reconstruct a model of the observed tooth to investigate whether intra-dental lesion could be observed without imaging the lesion directly.

To combine the images, different methods were attempted to reconstruct the composite image from multiple flat views.

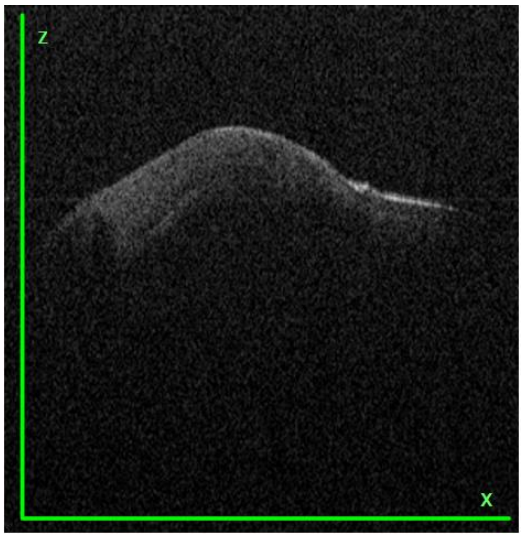

Figure 17 A single B-scan; the rotating stage rotates the tooth around the x-axis

Figure 18 A "face" scan is composed by a section of 500 B-scans taken along the y Axis

3.3 Image reconstruction with MATLAB

3.3.1.1 Rotation Reconstruction

Reconstructing the theta-stack made use of the information gathered by the instrument used (e.g. angle, height of A-scan, A-scans per B-scan, etc).

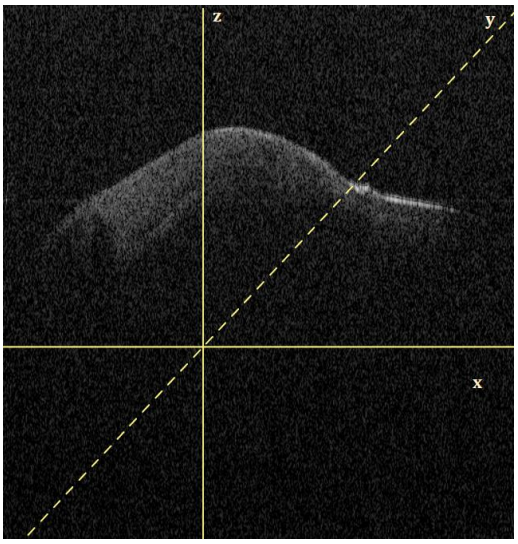

Figure 19 show the 3-dimensional plane with respect to a single B-scan; the stage rotated the tooth around the x-axis

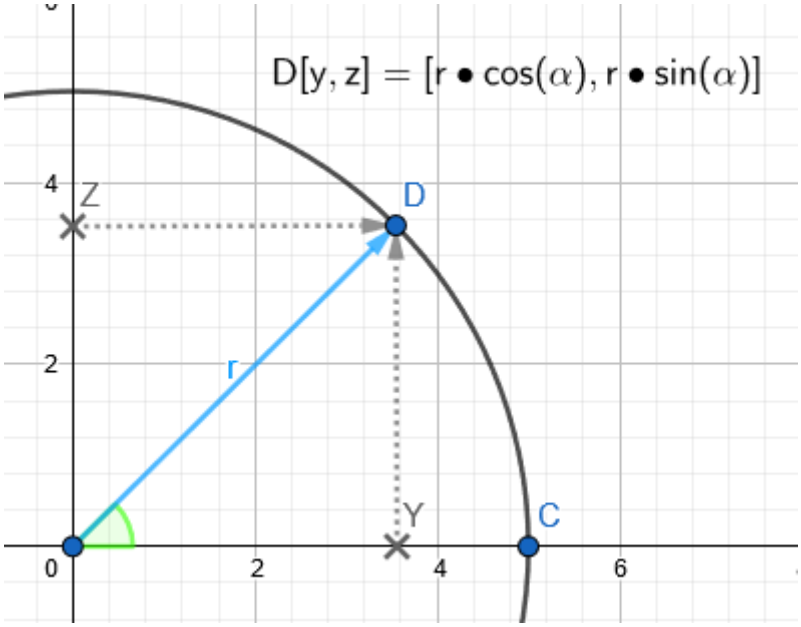

Figure 20 The coordinates of point C rotated by α around the x-axis [0,0], are given by $D[y,z] = [r \cdot cos\,\alpha\,, r \cdot sin\,\alpha]$, where r is the offset of point C from the rotation centre. Image created with GeoGebra (International GeoGebra Insitute, 2019).

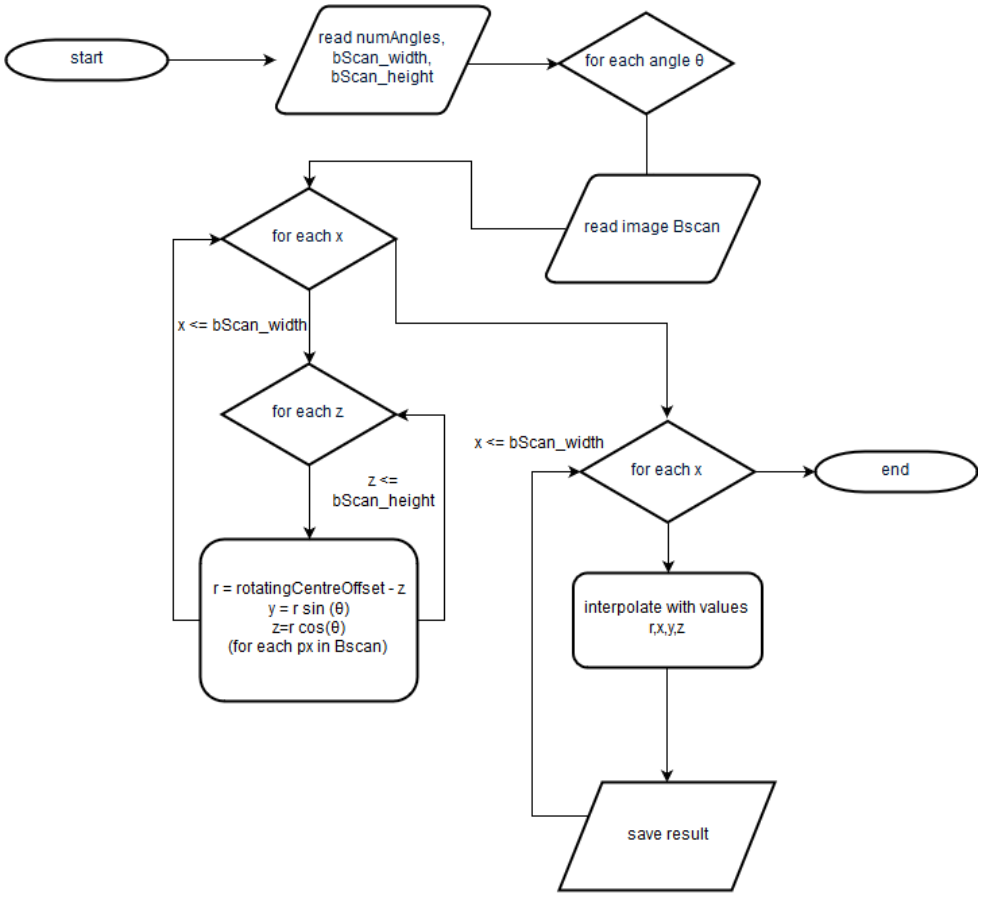

Figure 21 flowchart for theta-stack reconstruction (see 5.5)

3.4 Image registration with MATLAB

In any clinical setting, reconstructing images should require as little input as possible to be practical. For this reason, image registration techniques were investigated.

3.4.1.1 Intensity Based

In MATLAB's *Image Processing and Computer Vision Toolbox* (MathWorks, 2019) two main methods are available for 3-dimensional images natively: *Monomodal*, and *Multimodal*. Each has one optimizer and one error metric.

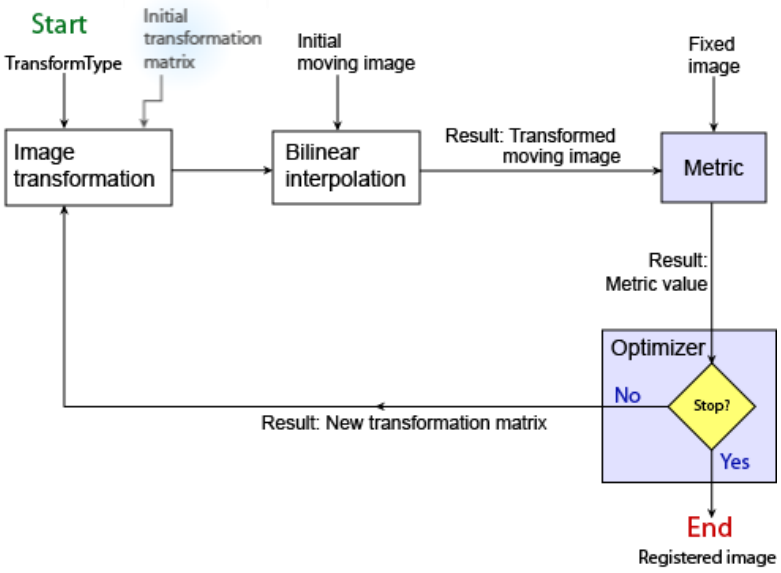

Figure 22 Intensity-based automatic registration in MATLAB flowchart (MathWorks, 2019)

The *monomodal* method supports only the use of simpler techniques (*gradient descent* algorithm and *means squared error*). The *multimodal* method implements *Mattes mutual information* metric and *One-plus-one evolutionary* optimization only. (MathWorks, 2019)

The function used to perform the registration is `imregister`; it takes two input images (a fixed acting as reference and a moving one) and returns a registered image with the resulting geometric transformation applied. It also allows to add additional parameters such as spatial referencing objects for both images, an object describing the initial transformation of the moving image, the maximum number of pyramids to be used and the type of geometric transformation to be applied to the moving image. (MathWorks, 2019)

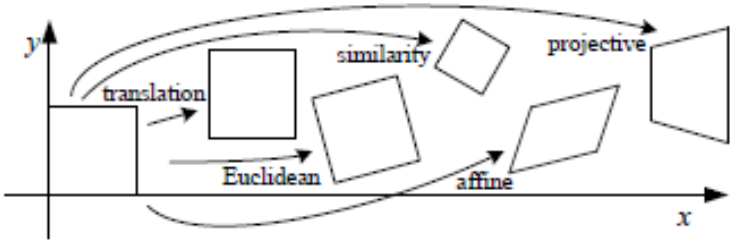

Figure 23 Basic set of 2D planar transformations (Szeliski, 2006)

Both methods were attempted, but it was observed that multimodal registration, while more expensive in terms of time and resource did not provide better results than monomodal registration.

3.4.1.2 Control Points selection

MATLAB's *Image Processing and Computer Vision Toolbox* also includes a Control Points selection tool, although it only works for 2-dimensional images. The tool allows the user to choose a series of common points between to images to estimate a geometric transformation.

An attempt was made to use this tool (Figure 14), based on the hope that it could be used to map two transformations to be applied consecutively to the volume (first on one plane, then the other). This was however abandoned due to the difficulty in aligning even two parts (occlusal and one of the faces in the image below) which have almost an entire surface in common.

Additionally, it was realized that there was no guarantee that the "plane of the tooth" would be aligned with the axis's in the volume object, and that there could be no transformation "at an angle" using this method and that the alternatives would render the results unviable (either applying a non-rigid transformation would "over-register" the image and modify warp the shape of the tooth, or keeping a rigid transformation would "under-register" the image)

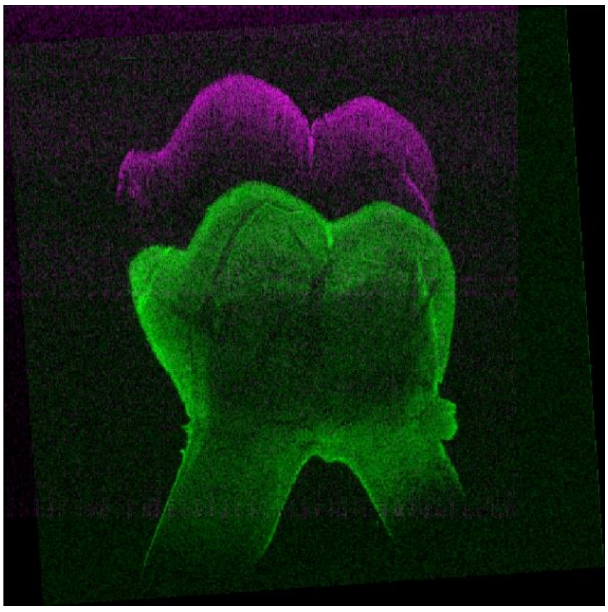

Figure 24 After an attempt to apply Control Points Registration along the x-y plane, the results were still "under-registered" and failed to match the chosen features.

3.5 Image quality

The only image significant "image quality feature" relevant to the scope of this project was the A-scan frequency rate. This was not investigated directly due to lack of time, but it was observed empirically by comparing the preliminary images (with a frequency of 500 Hz) to the remaining captured images (1kHz). A frequency of 1kHz was observed to be better suited to capturing finer details of the tooth structure.

3.6 Denoising

Although not the focus of this project, some experimentation was done with regards to denoising. This was done using Poisson-Gaussian denoising (Makitalo & Foi, 2012) (Maggioni, et al., 2014).

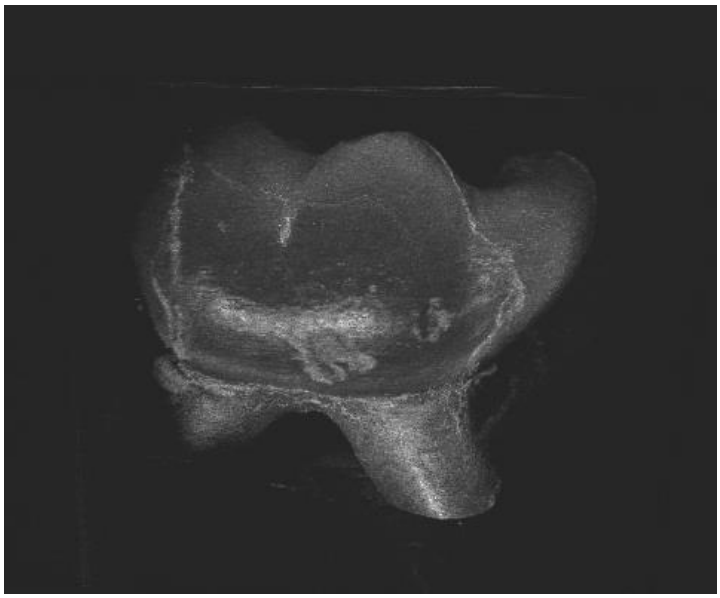

Figure 25 Denoised y-stack image

This was not pursued further since denoising was shown not to affect the quality of the registration, and the quality of the reconstruction.

3.7 Thresholding

Thresholding is an image-processing technique used to separate an object (foreground) from the background. (NIH, 2016)

Simple thresholding was applied to images.

Snippet 2 Thresholding code in loadOCT.m

```
% threshold the image
if (strcmp(varargin{3},'threshold'))
   % !note that if denoising volume is now double not uint8 so
   % threshold needs to be adjusted
    if(strcmp(varargin{3}, 'denoise'))
        threshold = varargin{4}/255;
    else
        threshold = varargin{4};
    end
    volume(volume<=threshold)=0;
end
```

While thresholding per-se did not affect the registration, it did help in observing the 3D volume and therefore was very useful during the pre-processing steps.

3.8 Comparisons with other imaging techniques

To evaluate the quality of the resulting reconstructed images, images were taken of the same tooth using other imaging techniques.

Figure 26 Clinical use of a DIAGNOcam (Ogodescu, et al., 2017)

3.8.1 DIAGNOcam comparison

DIAGNOcam uses another transillumination (see section 2.3.2 and section 2.3.2.1). Because the DIAGNOcam is designed to work in clinical settings, some adjustments had to be made to use it with the sample teeth.

This is because in clinical settings the light is fed through the gums into the tooth to avoid glare (visible in **Error! Reference source not found.**) and noise formation. To achieve this s ame "effect" in a lab setting, initially the light source was fed through the fingertip holding the tooth and later the tooth was embedded in a material with similar optical properties to the gingiva.

In these images the "lesion of interest" is visible as a darker area on one of the proximal sides (see **Error! Reference source not found.**).

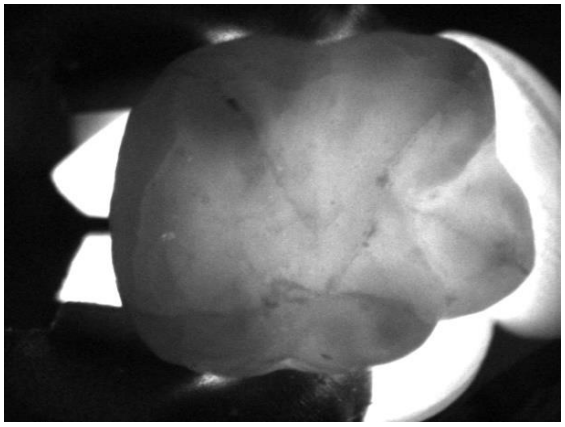

Figure 27 Proximal view of X1ba taken with the DIAGNOcam

Figure 28 Occlusal view of X1ba taken with the DIAGNOcam

3.8.2 X-Ray micro-CT comparison

A reference image was taken using X-Ray micro tomography (see 2.3.1.1). As X-Rays are fully penetrative, the image in a full depth representation contrary to what can be achieved using OCT.

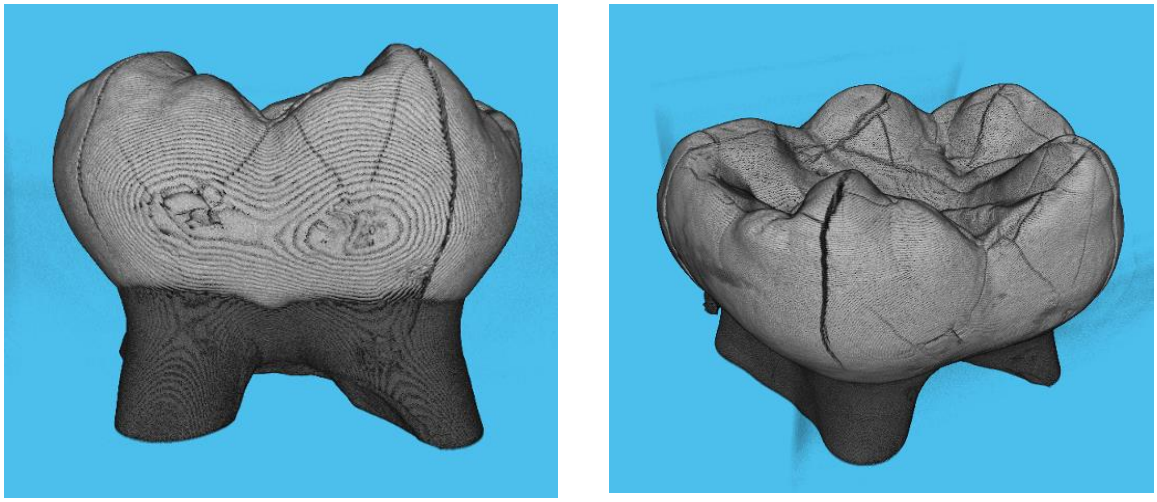

Figure 29 Images captured using X-ray CT

4 RESULTS AND ANALYSIS

4.1 Preliminary images of X1ba

The first step was to process some images of the tooth identified as 'X1ba' gathered at 500kHz without the use of the rotating stage but by rotating the tooth manually.

X1Ba presents a lesion in the proximal side which would be impossible to image directly using OCT in vivo. The lesion is superficial and is not clearly visible in the X-Ray image (Figure 30), but it is noticeable in the transillumination image taken by the DIAGNOcam (Figure 27).

Figure 30 X-Ray image of the proximal side (with lesion) of X1ba

4.1.1 Initial attempt

In the first attempt at a reconstruction, the images from different sides were simply loaded into MATLAB.

During this step, the biggest challenge was that, since the tooth had been moved manually, the images were extremely misaligned (see Figure 31 and Figure 32) and there was no consistent frame of reference.

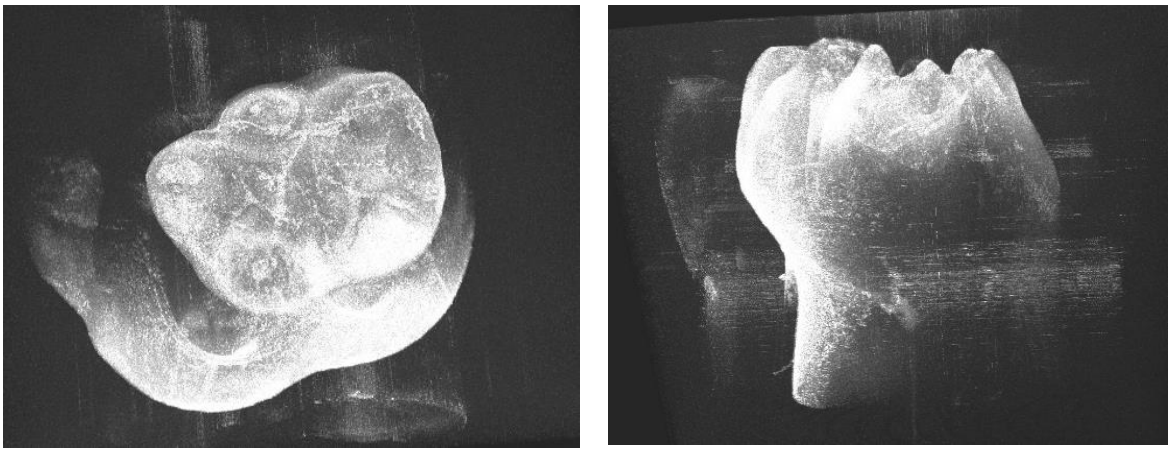

Figure 31 Reconstructed image shows misalignment of individual images (occlusal view)

Figure 32 Reconstructed image shows misalignment of individual image(proximal view)

The individual views were adjusted manually (rotation and scale) and then added into a single volume. After some trial and error, a composite image was obtained.

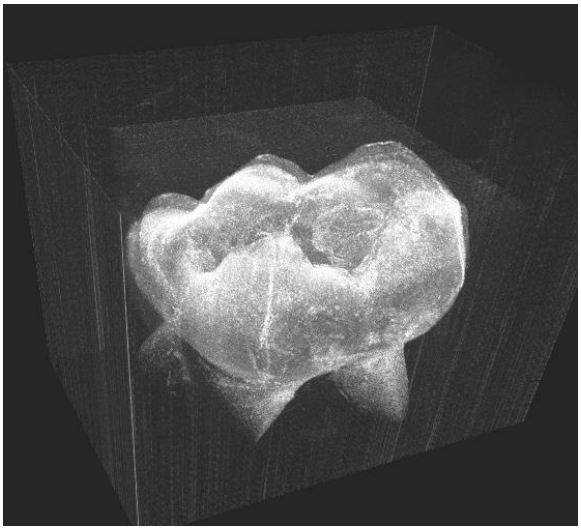

Figure 33 Manually reconstructed X1ba

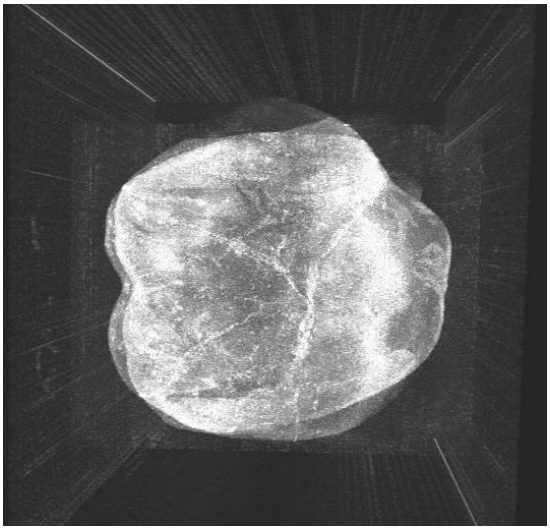

Figure 34 Manually reconstructed X1ba (occlusal view)

In this first reconstructed image, the lesion on the proximal side was not readily apparent.

Figure 35 Reconstructed X1ba (proximal side with lesion)

4.1.2 **Direct OCT image of the lesion**

For reference a 3D reconstruction of the proximal side with the lesion (circled red in Figure 36) was also used. The lesion does not appear as clearly as it does in images taken with transillumination (**Error! Reference source not found.**).

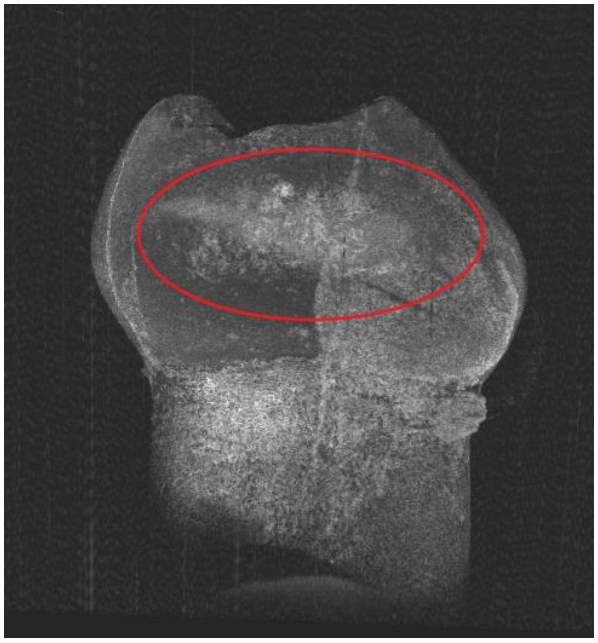

Figure 36 OCT reconstruction of the proximal view (lesion circled in red)

4.1.3 **Automatic registration of images**

However, because the images to be registered are all partial views of a tooth (thus have few points in common), and because the different views of the teeth are quite similar (i.e. similar shapes), the results of applying intensity-based automatic registration directly without any pre-processing are not good (

Figure 44).

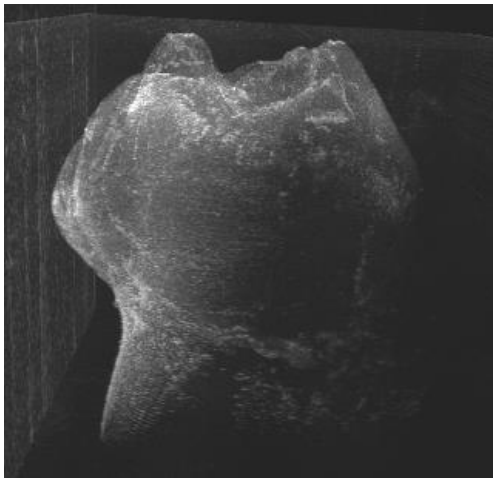

Figure 37 Intensity based registration without initial alignment (lateral view)

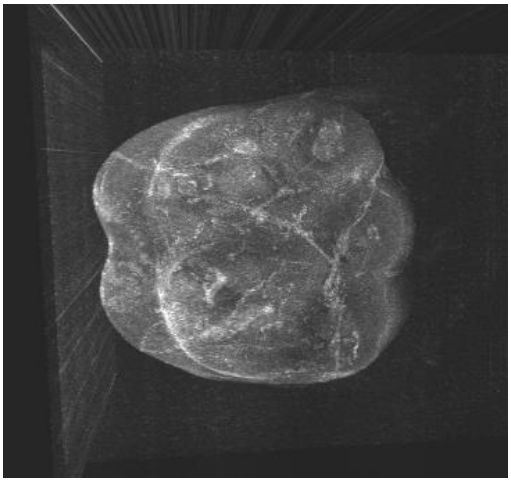

Figure 38 Intensity based registration without initial alignment (occlusal view)

However, applying the same transformations as in 4.1.1, and then using automatic registration before adding the images, yields better results.

It was noted that the only type of registration yielding good results was using *'translation'* transformation parameter; *'rigid'* transformation, was only successful when the rotation transformation was performed in the first step, essentially negating the rotation part of the parameter.

Other types of transformation allowed as parameters were not useful as they allowed the algorithm to reach a minimum too easily by misaligning the images.

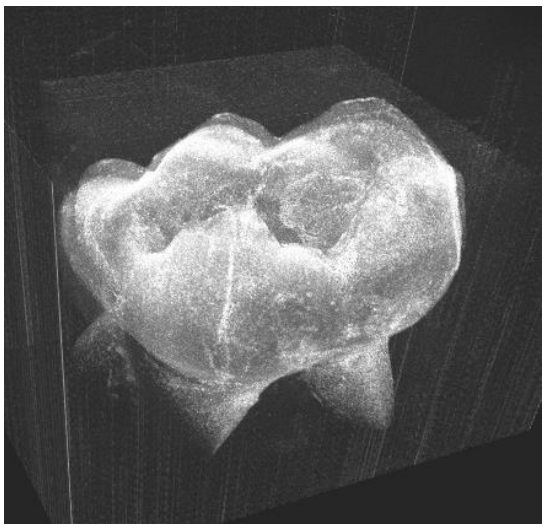

Figure 39 Intensity based registration after initial alignment

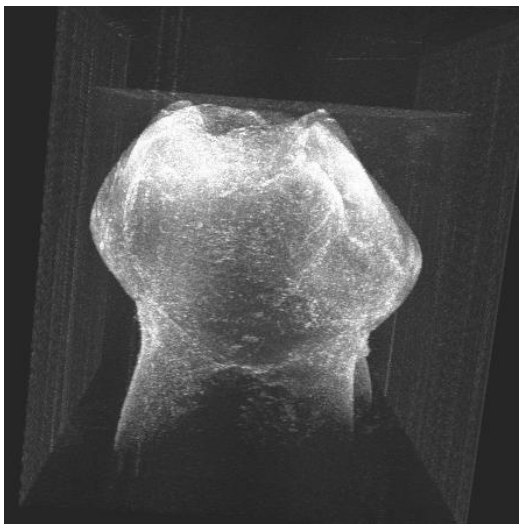

Figure 40 Intensity based registration after initial alignment (proximal side); lesion is still not clearly visible

4.2 Single B-scan Rotation

The image captured with a single B-scan per degree interval was sampled allowing only a partial angle from the buccal and lingual sides to mimic the angle of the reachable surface of a tooth in a mouth. The angles applied were from 90 degrees to 150 degrees.

As can be observed from the images below, no part of the proximal sides can be seen with an angle of 90 degrees. A shadow of what is (most likely) a lesion is visible in the 120-degrees image; however this is not very clear: a dentist might or might not be able to unequivocally identify that as a lesion.

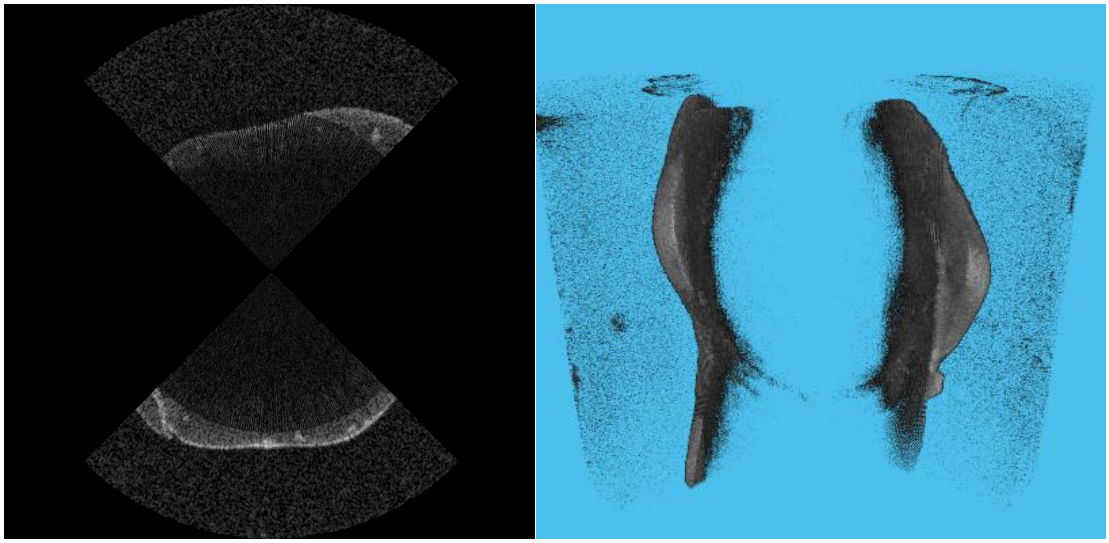

Figure 41 Theta-stack at 90 degrees

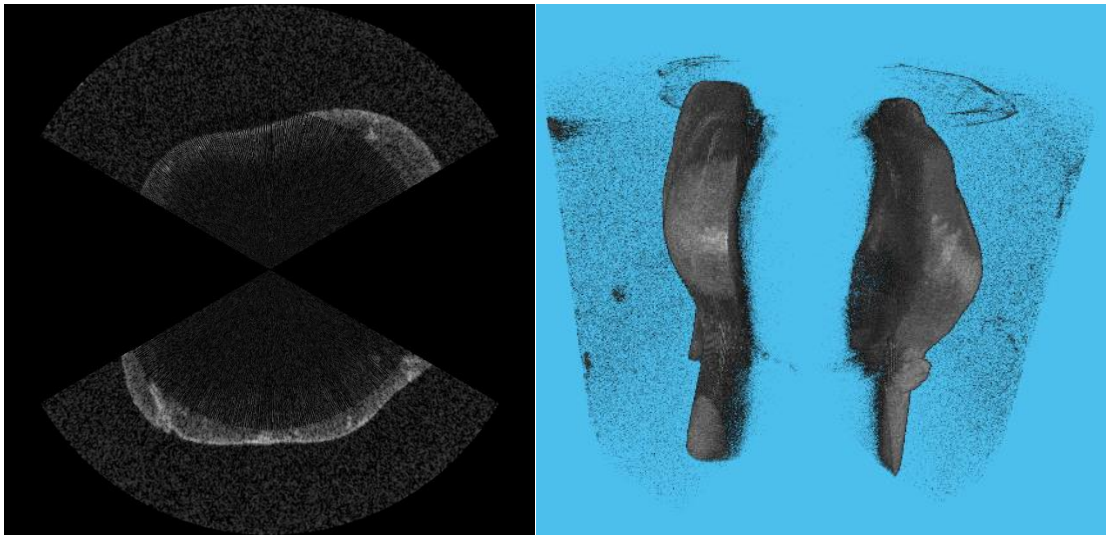

Figure 42 Theta-stack at 120 degrees

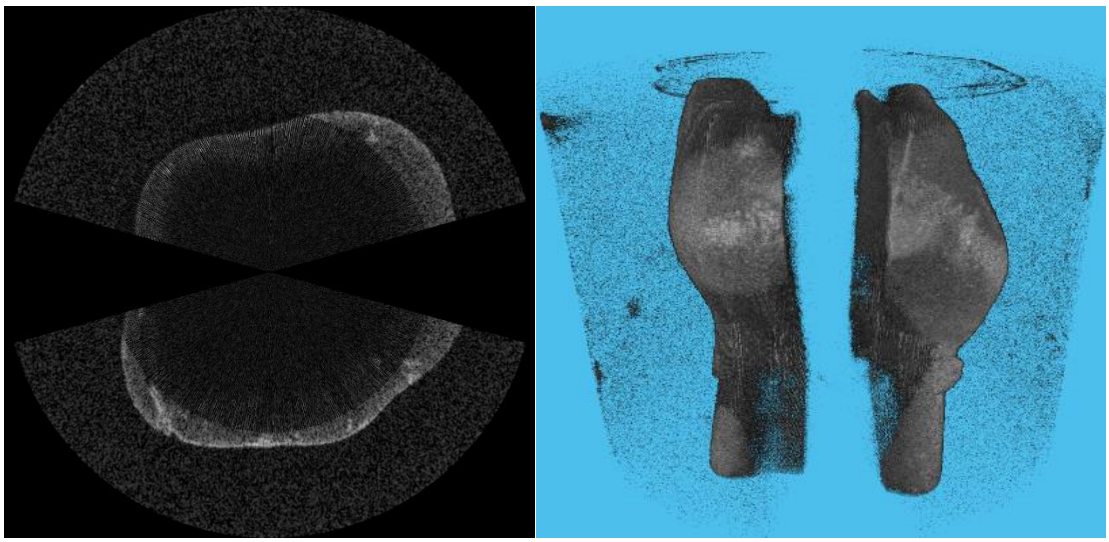

Figure 43 Theta-stack at 150 degrees

In the 150-degree image, a larger part of the lesion is clearly visible, even though a missing slice remains in the middle of the tooth.

4.3 Flat-views with multiple B-scans

The best results at both creating a 3-dimensional model and at automatic registration where achieved using the y-stack images. These images were more similar to the preliminary ones, but were also captured rotating the stage electronically at $\pm 40°$ from each face (i.e. 45, 90, 135 degrees and 225, 270, 315 degrees) which provided a stable reference for the initial alignment (Figure 45).

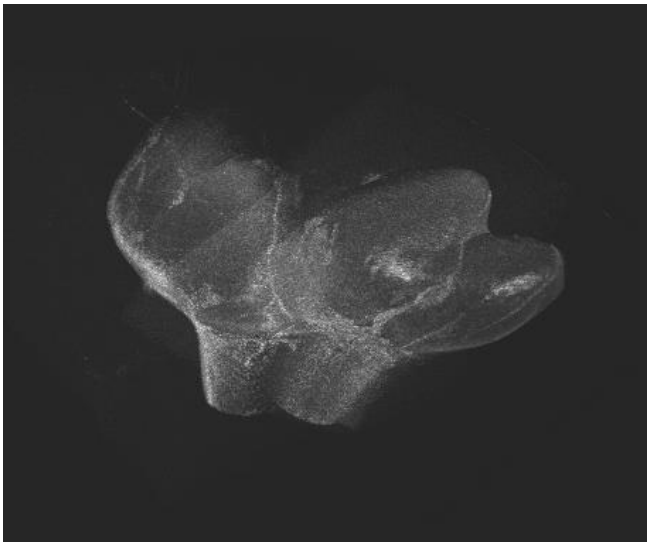

Figure 44 Intensity based registration without initial alignment

Pre-processing the image was still crucial, as it is very easy for the algorithm to find a bad minimum cost if allowed to rotate the image freely.Figure 44

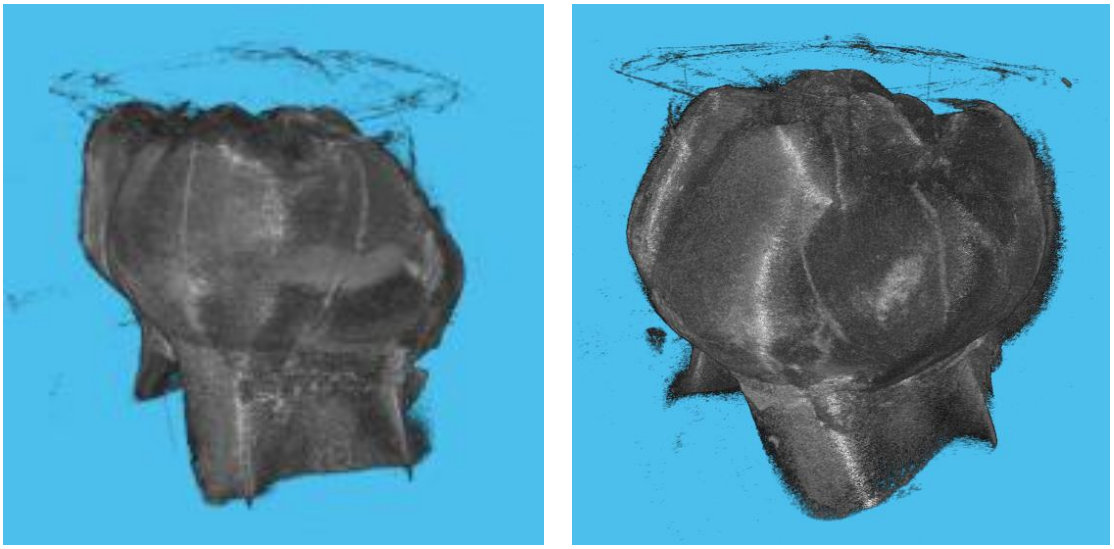

Figure 45 Initial alignment of the y-stack model

Snippet 3 Initial alignment of y-stacks performed around the rotation centre offset along the z-axis

```
offset = [0 -380 0];

[buccal_, buccal_ref_] = imtranslate(buccal, buccal_ref, offset,'OutputView', 'same');
[view45_, view45_ref_] = imtranslate(view45, view45_ref, offset,'OutputView', 'same');
[view135_, view135_ref_] = imtranslate(view135, view135_ref, offset,'OutputView', 'same');

[lingual_, lingual_ref_] = imtranslate(lingual, lingual_ref, offset,'OutputView', 'same');
[view225_, view225_ref_] = imtranslate(view225, view225_ref, offset,'OutputView', 'same');
[view315_, view315_ref_] = imtranslate(view315, view315_ref, offset,'OutputView', 'same');

view45_  = imrotate3(view45_, 45, [1 0 0], 'crop');
view135_ = imrotate3(view135_, 315, [1 0 0], 'crop');

lingual_  = imrotate3(lingual_, 180, [1 0 0], 'crop'); % loose | crop
view225_ = imrotate3(view225_, -135, [1 0 0], 'crop');
view315_ = imrotate3(view315_, 135, [1 0 0], 'crop');

volA = buccal_ + view45_ + view135_;
volB = lingual_ + view225_ + view315_;
volume_unreg = volA + volB;

saveAsPNGstack(volume_unreg,root_dir,"2204_unreg");
```

After the single y-stack images were rotated around the offset x-axis, the y-stacks were already close to be aligned. At this point the automatic registration was applied to fine-tune the alignment results.

Snippet 4 Monomodal registration performed to y-stack

```
[optimizer, metric] = imregconfig('monomodal')
                                          % MaximumIterations — Maximum number of iterations
optimizer.MaximumIterations = 500             % 100 (default) | positive integer scalar
                                          % GradientMagnitudeTolerance — Gradient magnitude tolerance
optimizer.GradientMagnitudeTolerance = 1e-8   % 1e-4 (default) | positive scalar
                                          % MinimumStepLength — Tolerance for convergence
optimizer.MinimumStepLength = 1e-7            % 1e-5 (default) | positive scalar
                                          % MaximumStepLength — Initial step length
optimizer.MaximumStepLength = 0.0625          % 0.0625 (default) | positive scalar
                                          % RelaxationFactor — Step length reduction factor
optimizer.RelaxationFactor = 0.2              % 0.5 (default) | positive scalar between 0 and 1

% 'rigid' or 'translation'
[view135_, view135__ref_] = imregister(view135_, view135_ref_, buccal_, buccal_ref, 'rigid', optimizer, metric);
[view45_, view45_ref_] = imregister(view45_, view45_ref_, buccal_, buccal_ref_, 'rigid', optimizer, metric);

volA_reg =  view45_ + buccal_ + view135_;
saveAsPNGstack(volA_reg,root_dir,"2204_regA");


[view225_, view225__ref_] = imregister(view225_, view225_ref_, lingual_, lingual_ref, 'rigid', optimizer, metric);
[view315_, view315__ref_] = imregister(view315_, view315_ref_, lingual_, lingual_ref_, 'rigid', optimizer, metric);

volB_reg =  view315_ + lingual_ + view225_;
saveAsPNGstack(volB_reg,root_dir,"2204_regB");
```

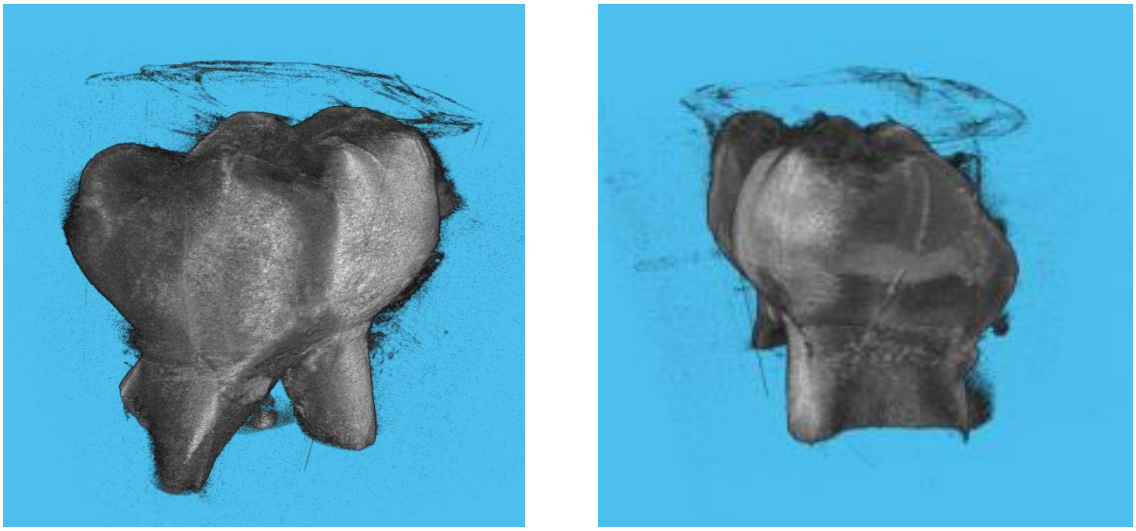

Figure 46 Registered y-stack reconstruction

5 CONCLUSIONS AND FUTURE WORK

5.1 Conclusions

5.1.1 Regarding the possibility of observing lesions by 3-dimensional reconstruction

There was a huge difference of what can be reconstructed from theta-stack vs from y-stack. As shown in

Figure 48 , y-stack offers a much wider coverage of the surface of the tooth (almost complete coverage of the proximal sides depending on shape of the tooth and distance between teeth).

On the other hand, theta-stack is limited to scanning right in front of the camera. This is a huge limitation especially if capturing images from the inside of the mouth or images of back-teeth. Moreover, as shown in section 4.2, the part not imaged cannot be reconstructed as it is completely “blacked out”.

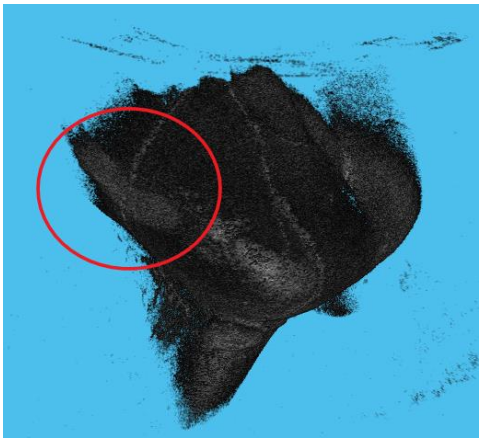

Figure 47 y-stack image at 45 degrees from the midline clearly displays the lesion as well as most of the proximal face of the tooth

Not only y-stack is better versed for reconstruction via multiple images, but a single well-placed y-stack image, can show most of the proximal side of a tooth as in Figure 47 (again, depending on shape of the tooth and distance between teeth).

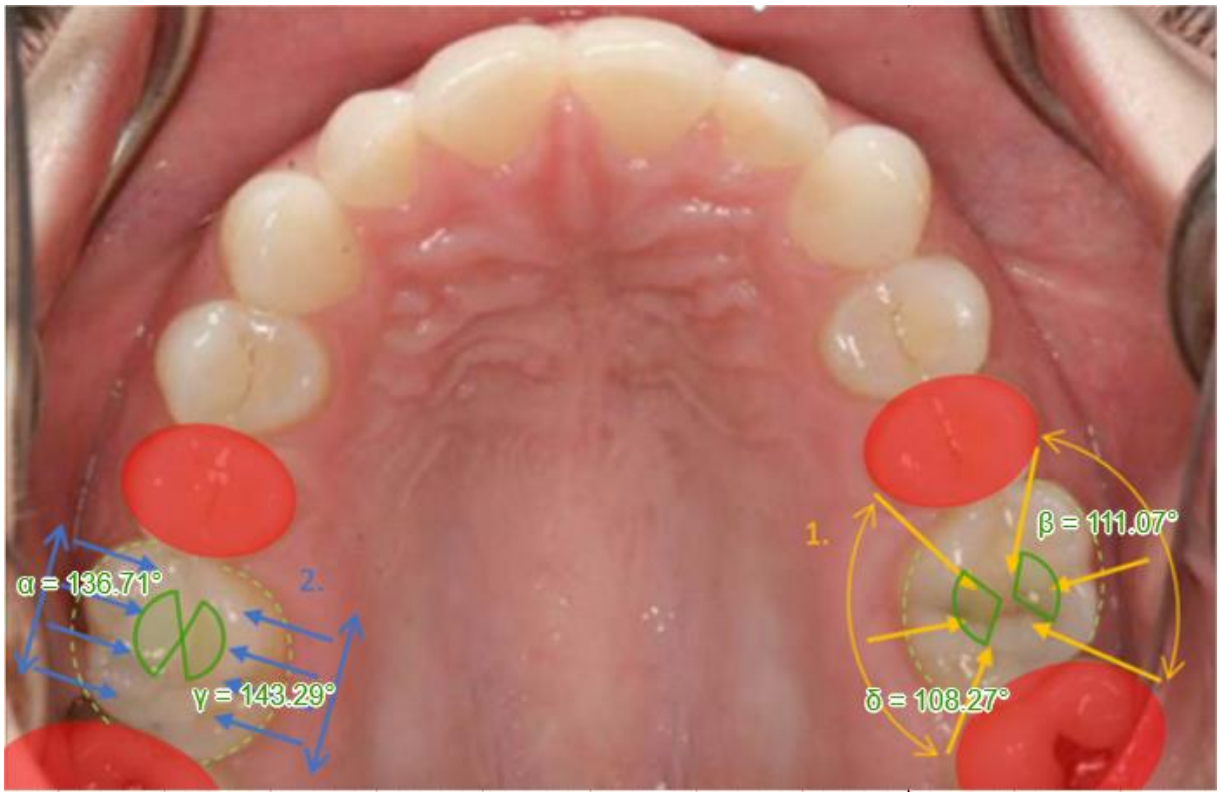

Figure 48 The surface coverage of the two main methods used; (1) Theta-stack, (2) Y-stack. Photo adapted image from: (Dental Arts Laboratories, Inc., n.d.) with the use of GeoGebra (International GeoGebra Insitute, 2019) for the angle measurements.

5.1.2 **Regarding the registration of images of teeth**

This project highlighted the difficulty related to registering images of teeth.

The biggest challenge is that the structures of a tooth are very similar in terms of shape and composition. This means that generic image registration algorithm can be easily confused into accepting a minimum which does not corresponds to a correct registration.

This was highlighted when attempting to use image registration without any pre-processing steps or when setting the parameter in the function to anything that allowed anything more than a translation.

Another challenge is that, because OCT images are not fully penetrative with respect of the tooth, the images to be registered have relatively little overlap for the algorithm to work with.

This is still a secondary problem, in my opinion, compared to the self-similarity of teeth structures, as more distinctive features could allow for registration even with little overlap.

Another point worth noting is that OCT images only have no “background” which might help with registration by providing a “reference“ in spite of the self-similarity of teeth structures.

Currently there was no algorithm which could register OCT teeth image to allow for a 3-dimensional reconstruction without significant pre-processing. Image registration remains crucial to any clinical application of OCT-based 3-dimensional reconstructions.

5.2 Future work

Better results could be achieved by using a different type of registration algorithm matches in some parts of the image over others.

For example, an approach to this could be to bias the algorithm for registration in favour of the tooth root since by aligning the root correctly would account for most of translation, rotation and resizing transformation which would otherwise be performed in pre-processing.

Anecdotally, the pre-processing performed throughout this project was done following this technique, as it is the easiest way to spot small amounts of misalignment.

This approach would require the algorithm to “know” which part of the image contains the tooth root, and this could be achieved either as a pre-processing task or using machine learning feature-detection.

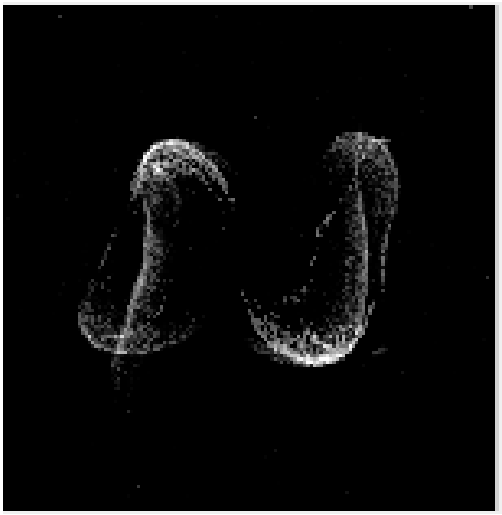

Figure 49 Section of an unregistered image

Another possible approach could be to implement a software allowing for 3-dimensional control points registration to allow manual alignment. However this could result in a difficult pre-processing step (especially if used with current registration methods which require a high level of harmonization in pre-processing to be useful) since it would involve picking multiple control points in 3-dimensions

BIBLIOGRAPHY

Merriam-Webster, n.d. *Lingual | Definition of Lingual by Merriam-Webster.* [Online]
Available at: https://www.merriam-webster.com/dictionary/lingual#medicalDictionary
[Accessed 18 March 2018].

Adelson, E. H. et al., 1984. *Pyramid methods in image processing.* [Online]
Available at: http://persci.mit.edu/pub_pdfs/RCA84.pdf
[Accessed 20 April 2019].

Ballantyne Endodontics, 2018. *Mesial of The Tooth: Understanding Dental Lingo.* [Online]
Available at: https://www.ballantyneendo.com/blog/mesial-of-the-tooth-understanding-dental-lingo/
[Accessed 18 March 2018].

Castellucci, A., 2005. A Brief History of Endodontics. In: *Endodontics.* s.l.:Il Tridente, pp. 2-5.

Children's Dentistry of North Las Vegas, n.d. *Children's Dental X-Rays.* [Online]
Available at: https://childrensedationdentist.com/childrens-dental-x-rays/
[Accessed 6 December 2018].

Cooperative Institute for Meteorological Satellite Studies Space Science and Engineering Center (SSEC), University of Wisconsin-Madison, n.d. *What is Matlab.* [Online]
Available at: https://cimss.ssec.wisc.edu/wxwise/class/aos340/spr00/whatismatlab.htm
[Accessed 6 December 2018].

Dental Arts Laboratories, Inc., n.d. *DAL Signature Recommended Photo Records.* [Online]
Available at: http://www.dentalartslab.com/dal-signature-restorations/resources/dal-signature-recommended-photo-records/
[Accessed 22 April 2019].

Encyclopædia Britannica, Inc., n.d. *Coherence.* [Online]
Available at: https://www.britannica.com/science/coherence
[Accessed 6 December 2018].

Encyclopaedia Britannica, Inc., n.d. *Critical Angle.* [Online]
Available at: https://www.britannica.com/science/critical-angle
[Accessed 6 December 2018].

Encyclopaedia Britannica, Inc., n.d. *Reflection (Physics).* [Online]
Available at: https://www.britannica.com/science/reflection-physics
[Accessed 6 December 2018].

Encyclopædia Britannica, Inc., n.d. *Refraction.* [Online]
Available at: https://www.britannica.com/science/refraction
[Accessed 6 December 2018].

Encyclopaedia Britannica, Inc., n.d. *Snell's Law.* [Online]
Available at: https://www.britannica.com/science/Snells-law
[Accessed 6 December 2018].

Erten, O. & Yimlaz, B. N., 2018. Three-Dimensional Imaging in Orthodontics. *Turkish Journal of Orthodontics,* Volume 31, pp. 86-94.

Gabriele, M. L. et al., 2011. Optical Coherence Tomography: History, Current Status, and Laboratory Work. *Investigative Ophtalmology & Visual Science,* 52(5), pp. 2425-2436.

Georgia State University, n.d. *Michelson Interferometer.* [Online]
Available at: http://hyperphysics.phy-astr.gsu.edu/hbase/phyopt/michel.html
[Accessed 30 November 2018].

Hai-ping Ren, H. Y. W.-k. W., 2001. *Multi-resolution three-dimensional multi-modality Image Registration by Maximization of Mutual Information.* Istambul, Turkey, Proceedings of the 23rd Annual EMBS International Conference.

Huang, D. et al., 1991. Optical Coherence Tomography. *Science,* 254(5035), pp. 1178-1181.

International GeoGebra Insitute, 2019. *Graphing Calculator - GeoGebra.* [Online]
Available at: https://www.geogebra.org/graphing
[Accessed 23 April 2019].

KaVo Dental, n.d. *KaVo Dental.* [Online]
Available at: https://www.kavo.com/
[Accessed 6 December 2018].

Maggioni, M. et al., 2014. *Image and video denoising by sparse 3D transform-domain collaborative filtering | Block-matching and 3D filtering (BM3D) algorithm and its extensions.* [Online]
Available at: http://www.cs.tut.fi/~foi/GCF-BM3D/
[Accessed 25 January 2019].

Makitalo, M. & Foi, A., 2012. *Poisson-Gaussian Denoising using the exact unbiased inverse of the generalized anscombe transformation.* [Online]
Available at: http://www.cs.tut.fi/~foi/papers/ICASSP2012-Makitalo-Foi-GenAnscombe.pdf
[Accessed 25 January 2019].

MathWorks, 2019. *Create an Optimizer and Metric for Intensity-Based Image Registration.* [Online]
Available at: https://uk.mathworks.com/help/images/create-an-optimizer-and-metric-for-intensity-based-image-registration.html
[Accessed 22 April 2019].

MathWorks, 2019. *Image Processing Toolbox™ Reference.* [Online]
Available at: https://uk.mathworks.com/help/pdf_doc/images/images_ref.pdf
[Accessed 5 April 2019].

MathWorks, 2019. *imregister.* [Online]
Available at: https://uk.mathworks.com/help/images/ref/imregister.html#btcaexy-1-transformType
[Accessed 21 April 2019].

MathWorks, 2019. *Intensity-Based Automatic Image Registration.* [Online]
Available at: https://uk.mathworks.com/help/images/intensity-based-automatic-image-registration.html
[Accessed 20 April 2019].

MathWorks, 2019. *Mean Square Error Configuration.* [Online]
Available at:
https://uk.mathworks.com/help/images/ref/registration.metric.meansquares.html
[Accessed 22 April 2019].

MathWorks, n.d. *Images in MATLAB.* [Online]
Available at: https://uk.mathworks.com/help/images/images-in-matlab.html
[Accessed 2019 April 21].

MathWorks, n.d. *Vectorization.* [Online]
Available at: https://www.mathworks.com/help/matlab/matlab_prog/vectorization.html
[Accessed 20 March 2018].

Merriam-Webster, Incorporated, n.d. *Occlusal | Definition of Occlusal by Merriam-Webster.* [Online]
Available at: https://www.merriam-webster.com/dictionary/occlusal#medicalDictionary
[Accessed 18 March 2018].

Merriam-Webster, n.d. *Buccal | Definition of Buccal by Merriam-Webster.* [Online]
Available at: https://www.merriam-webster.com/dictionary/buccal#medicalDictionary
[Accessed 18 March 2018].

Merriam-Webster, n.d. *Occlusal Plane Medical Definition | Merriam-Webster Medical Dictionary.* [Online]
Available at: https://www.merriam-webster.com/medical/occlusal%20plane
[Accessed 18 March 2018].

Merriam-Webster, n.d. *Proximal | Definition of Proximal by Merriam-Webster.* [Online]
Available at: https://www.merriam-webster.com/dictionary/proximal#medicalDictionary
[Accessed 18 March 2018].

NASA, n.d. *X-ray Micro-Tomography (micro-CT).* [Online]
Available at: https://data.nasa.gov/Aerospace/X-ray-Micro-Tomography-micro-CT-/f7qz-8dsr
[Accessed 18 March 2018].

NIH, 2016. *Thresholding - ImageJ.* [Online]
Available at: https://imagej.net/Thresholding
[Accessed 20 April 2019].

OCT lab at Queen Mary University of London, 2016. *OCTview-lab,* London: Queen Mary University of London.

Ogodescu, A., Andreea, I., Ogodescu, E. & Magda, L., 2017. Unconventional Non-Invasive Diagnostic Techniques and Treatment of White Spot Lesions in Paediatric Dentistry and Orthodontics. *European Scientific Journal,* 13(15), pp. 1857-7881.

Optical and Biomedical Engineering Laboratory, University of Western Australia, n.d. *Introduction to OCT - OBEL.* [Online]
Available at: http://obel.ee.uwa.edu.au/research/fundamentals/introduction-oct/
[Accessed 3 December 2018].

Paschotta, D. R., n.d. *Optical Heterodyne Detection.* [Online]
Available at: https://www.rp-photonics.com/optical_heterodyne_detection.html
[Accessed 6 December 2018].

Popescu, D. P. et al., 2011. Thorlabs, Inc. - Your Source for Fiber Optics, Laser Diodes, Optical Instrumentation and Polarization Measurement & Control. *Biophysical reviews,* 6 August, 3(3), pp. 155-169.

Popescu, P. G., n.d. *Low Coherence Interferometry.* [Online]
Available at: http://light.ece.illinois.edu/ECE460/PDF/LCI.pdf
[Accessed 6 December 2018].

Shah, N. e. a., 2014. Recent advances in imaging technologies in dentistry. *World journal of radiology,* 6(10), pp. 794-807.

Shure, L., 2016. *Run Code Faster With the New MATLAB Execution Engine.* [Online]
Available at: https://blogs.mathworks.com/loren/2016/02/12/run-code-faster-with-the-new-matlab-execution-engine/#a10b1355-2da4-47e8-87b9-bac247d0b6a6
[Accessed 20 March 2019].

Studio dentistico associato Fazi Colangelo, n.d. *Diagnocam by Kavo.* [Online]
Available at: https://www.dentistafirenze.com/en/tecnologie-diagnocam.asp
[Accessed 6 December 2018].

Szeliski, R., 2006. *Microsoft Research – Emerging Technology, Computer, and Software Research.* [Online]
Available at: http://www.research.microsoft.com
[Accessed 10 March 2019].

ThorLabs, Inc., n.d. *OCT Systems Tutorials.* [Online]
Available at: https://www.thorlabs.com/newgrouppage9.cfm?objectgroup_id=10763
[Accessed 3 Decembrer 2018].

U.S. Food and Drug Administration, 2018. *Medical X-ray Imaging.* [Online]
Available at: https://www.fda.gov/Radiation-EmittingProducts/RadiationEmittingProductsandProcedures/MedicalImaging/MedicalX-

Rays/default.htm#manufacturers
[Accessed 18 March 2019].

wikimedia.org, n.d. *Principle-TD-FD_OCT.* [Online]
Available at: https://upload.wikimedia.org/wikipedia/commons/d/d8/Principle-TD-FD_OCT.svg
[Accessed 2 December 2018].

APPENDICES

5.3 loadOCT.m

```
% uses the BM3D by Kostadin Dabov, Aram Danieyan,
% Alessandro Foi; found at
% http://www.cs.tut.fi/~foi/GCF-BM3D

function [volume, varargout] = loadOCT(path, varargin)
%   loadOCT(path, 'threshold', clean_factor, 'imref', [xref, yref, zref]) :
Load the 3D image from a stack of png
%       imref is real-world coordinates can be used to register the image
%       threshold is the threshold to hide all pixels with a value smaller
%

str = strcat(path, '\*.png')
D = dir(str)

% read the image
for i = 1:numel(D)
  tmp_path = strcat (D(i).folder, '\', D(i).name);
  tmp = imread(tmp_path);
  if (size(tmp ,3) == 3)
    tmp = squeeze(rgb2gray(tmp));
  end
  if (i==1)
      volume = zeros(size(tmp,1),size(tmp,2),0);
  end
  volume = cat(3,volume, tmp);
end


if(nargin>1)
    % imref3d obj is created for real-world coords to help in
    if (strcmp(varargin{1}, 'imref') && size(varargin{2},2)==3)
        varargout{1} = imref3d(size(volume), varargin{2}(1),
varargin{2}(2), varargin{2}(3));
    end

    if(nargin>3)
        if (nargin > 5)
           % in the case both 'denoise' & 'threshold' are set,
           % the thresholding is done after denoising
           if (strcmp(varargin{3}, 'denoise'))
                randn('seed', 0);
                sigma = varargin{4};
```

```
                volume = im2double(volume);
                z = volume + (sigma/255)*randn(size(volume));
                for i = 1:size(z,2)
                [NA, volume(:,i,:)] = BM3D(1, squeeze(z(:,i,:)), sigma);
            end
           end
        % threshold the image
        if (strcmp(varargin{3},'threshold'))
           % !note that if denoising volume is now double not uint8 so
           % threshold needs to be adjusted
            if(strcmp(varargin{3}, 'denoise'))
                threshold = varargin{4}/255;
            else
                threshold = varargin{4};
            end
            volume(volume<=threshold)=0;
        end
    end
end

end
```

5.4 Y-stack script

```
% Uses Image Processing & Computer vision toolbox for MATLAB
% https://www.mathworks.com/solutions/image-video-processing.html

uses the BM3D by Kostadin Dabov, Aram Danieyan,                          %
Alessandro Foi; found at
% http://www.cs.tut.fi/~foi/GCF-BM3D


clear all;
root_dir % path to folder with image stacks to be assigned

%%
threshold = 70    %for image thresholding
sigma = 25        %for denoising

z_PixelSize=20.2712; % microns per pixel
x_PixelSize=10.3425; % microns per pixel
y_PixelSize=13.3867; % microns per pixel

imref = [x_PixelSize z_PixelSize y_PixelSize];

[buccal, buccal_ref] = loadOCT(composePath(root_dir,'1kHz_Buccal'),'imref',
imref, 'clean',threshold, 'denoise', sigma);
[lingual, lingual_ref] =
loadOCT(composePath(root_dir,'1kHz_Lingual'),'imref', imref,
'clean',threshold, 'denoise', sigma);
[view45, view45_ref] =
loadOCT(composePath(root_dir,'1kHz_Proximal_noLesion_45'),'imref', imref,
'clean',threshold, 'denoise', sigma);
[view135, view135_ref] =
loadOCT(composePath(root_dir,'1kHz_Proximal_noLesion_135'),'imref', imref,
'clean',threshold, 'denoise', sigma);
```

```
[view225, view225_ref] =
loadOCT(composePath(root_dir,'1kHz_Proximal_Lesion_225'),'imref', imref,
'clean',threshold, 'denoise', sigma);
[view315, view315_ref] =
loadOCT(composePath(root_dir,'1kHz_Proximal_Lesion_315'),'imref', imref,
'clean',threshold, 'denoise', sigma);

%%
offset = [0 -380 0];          % rotation offset

[buccal_, buccal_ref_] = imtranslate(buccal, buccal_ref,
offset,'OutputView', 'same');
[view45_, view45_ref_] = imtranslate(view45, view45_ref,
offset,'OutputView', 'same');
[view135_, view135_ref_] = imtranslate(view135, view135_ref,
offset,'OutputView', 'same');

[lingual_, lingual_ref_] = imtranslate(lingual, lingual_ref,
offset,'OutputView', 'same');
[view225_, view225_ref_] = imtranslate(view225, view225_ref,
offset,'OutputView', 'same');
[view315_, view315_ref_] = imtranslate(view315, view315_ref,
offset,'OutputView', 'same');

view45_  = imrotate3(view45_, 45, [1 0 0], 'crop');
view135_ = imrotate3(view135_, 315, [1 0 0], 'crop');

lingual_  = imrotate3(lingual_, 180, [1 0 0], 'crop'); % loose | crop
view225_ = imrotate3(view225_, -135, [1 0 0], 'crop');
view315_ = imrotate3(view315_, 135, [1 0 0], 'crop');

volA = buccal_ + view45_ + view135_;
volB = lingual_ + view225_ + view315_;
volume_unreg = volA + volB;

saveAsPNGstack(volume_unreg,root_dir,"2204_unreg");

%%
[optimizer, metric] = imregconfig('monomodal')
                                                % MaximumIterations —
Maximum number of iterations
optimizer.MaximumIterations = 500                   % 100 (default) |
positive integer scalar
                                                %
GradientMagnitudeTolerance — Gradient magnitude tolerance
optimizer.GradientMagnitudeTolerance = 1e-8         % 1e-4 (default) |
positive scalar
                                                % MinimumStepLength —
Tolerance for convergence
optimizer.MinimumStepLength = 1e-7                  % 1e-5 (default) |
positive scalar
                                                % MaximumStepLength —
Initial step length
optimizer.MaximumStepLength = 0.0625                % 0.0625 (default) |
positive scalar
                                                % RelaxationFactor — Step
length reduction factor
optimizer.RelaxationFactor = 0.2                    % 0.5 (default) |
positive scalar between 0 and 1
```

```
% 'rigid' or 'translation'
[view135_, view135__ref_] = imregister(view135_, view135_ref_, buccal_,
buccal_ref, 'rigid', optimizer, metric);
[view45_, view45_ref_] = imregister(view45_, view45_ref_, buccal_,
buccal_ref_, 'rigid', optimizer, metric);

volA_reg =  view45_ + buccal_ + view135_;
saveAsPNGstack(volA_reg,root_dir,"2204_regA");


[view225_, view225__ref_] = imregister(view225_, view225_ref_, lingual_,
lingual_ref, 'rigid', optimizer, metric);
[view315_, view315__ref_] = imregister(view315_, view315_ref_, lingual_,
lingual_ref_, 'rigid', optimizer, metric);

volB_reg =  view315_ + lingual_ + view225_;
saveAsPNGstack(volB_reg,root_dir,"2204_regB");

%%
volume_reg = volA_reg + volB_reg;
saveAsPNGstack(volume_reg,root_dir,"2204_reg");

%%
volumeViewer(volume_unreg);
volumeViewer(volume_reg);
```

5.5 Theta-stack script

```
% Queen Mary University of London OCT Lab (kindly provided by Dr Tomlins)
% Reconstruct a 3D volume from OCT images obtained at multiple angles
% 16 January 2016
% 31 January - interpolate 2D planes, open data from mat file
%
% Febraury 2019 adapted to limited angle view

function loadRotatingOCT(path, rotationOffset, varargin)
%loadRotatingOCT Loads a theta-stack image
    % images are read from 'path' directory & new image is saved to 'path'
    % rotationOffset z pixel of axis of rotation
    % varargin{1}:  gamma "visible" angle
    % varargin{2}:  angle where non proximal face is

    % rotationOffset = 320; % rotation offset for theta_stack captured

    outputDir = strcat(path, '\3DReconstruction\');
    path = strcat(path, '\Repeat0000\');
    csv_path = strcat(path,'Position0000\parameters.csv');
    topDir = '\B-Scans\OCTImage0000.png';

    inputDir = dir(path)

    pxSize = [10.3425,20.2712, 13.3867]; % [x,z,y] - microns per pixel

    totalAngles = numel(inputDir) - 2;

    if nargin > 2
        delta = 360/totalAngles;
```

```
        gamma = [floor((varargin{2}-(varargin{1}/2))/delta)
ceil((varargin{2}+(varargin{1}/2))/delta); floor(((varargin{2}+180)-
(varargin{1}/2))/delta) ceil(((varargin{2}+180)+(varargin{1}/2))/delta)]
    else
        gamma = 0;
    end

    if ~exist(outputDir, 'dir')
        mkdir(outputDir);
    end

    bScan_width = dlmread(csv_path,',',[2,1,2,1]);    % tooth depth
    bScan_height = dlmread(csv_path,',',[6,1,6,1])/2; % tooth height

    volume = zeros(bScan_height,bScan_width,0);
    coords = zeros([bScan_height*bScan_width*totalAngles, 4]);

    n = 0;

    for i = 0:(totalAngles-1) % file names start at zero but array indices
at 1!
        bScan_path = strcat(path, sprintf('Position%04d', i));
        theta =
dlmread(strcat(bScan_path,'\parameters.csv'),',',[21,1,21,1]);

        tmp = imread(strcat(bScan_path, topDir));

        if(size(tmp ,3) == 3)
            tmp = squeeze(rgb2gray(tmp));
        end

        volume = cat(3,volume, tmp);

        for w = 1:bScan_width
            x = w*pxSize(1);

            for h = 1:bScan_height
                r = (rotationOffset - h)*pxSize(2);
                y = r*sin(theta*pi/180);
                z = r*cos(theta*pi/180);
                n = n+1;
%                 image values are NaN in areas outside gamma angle
                if (nargin > 2)% && ( ( (i<gamma(1,1)) && (i>gamma(1,2) ) )
|| ( (i<gamma(2,1)) && (i>gamma(2,2)) ) )
                    if (((i > gamma(1,1)) && (i < gamma(1,2)))||((i >
gamma(2,1)) && (i < gamma(2,2))))
                        coords(n,:) = [x, y, z, NaN];
                    else
                        coords(n,:) = [x, y, z, double(tmp(h,w))];
                    end
                else
                    coords(n,:) = [x, y, z, double(tmp(h,w))];
                end
            end
        end
    end

%     min_D=min(coords(:,2));
%     max_D=max(coords(:,2));
```

```
%     min_W=min(coords(:,3));
%     max_W=max(coords(:,3));
%
%     iwh = reshape(coords,[bScan_height,bScan_width,totalAngles,4]);
%     nPlane = bScan_height*totalAngles;
%
%     for w = 1:bScan_width
%         W = reshape(iwh(:,w,:,3),[nPlane,1]);
%         D = reshape(iwh(:,w,:,2),[nPlane,1]);
%         II = reshape(iwh(:,w,:,4),[nPlane,1]);
%
%         [grid_W, grid_D] =
meshgrid(min_W:pxSize(1):max_W,min_D,pxSize(1):max_D);
%         interpolatedGrid =
griddata(W,D,II,squeeze(grid_W),squeeze(grid_D),'linear');
%
%         img = uint16(interpolatedGrid);
%
%         imwrite(img, strcat(outputDir, sprintf('%04d',w), '.png'));
%     end

%     X=coords(:,1);
%     Y=coords(:,2);
%     Z=coords(:,3);
%     I=coords(:,4);

minD=min(coords(:,2));
maxD=max(coords(:,2));
minW=min(coords(:,3));
maxW=max(coords(:,3));
%
% Gather all coordinates in the same x plane (OCT coords) and interpolate
% onto a 2D regular grid
%
iwh=reshape(coords,[bScan_height,bScan_width,totalAngles,4]);
nPlane=bScan_height*totalAngles;

% pixelSize=pxSize(1);


for w=1:bScan_width % go to each vertical plane
    V=w;    % vertical coordinate;
    W=reshape(iwh(:,w,:,3),[nPlane,1]);  % Across the volume
    D=reshape(iwh(:,w,:,2),[nPlane,1]);     % Into the page
    II=reshape(iwh(:,w,:,4),[nPlane,1]);     % Into the page
    [gridW,gridD]=meshgrid(minW:pxSize(1):maxW,minD:pxSize(1):maxD);
    interpolatedGrid=griddata(W,D,II,gridW,gridD,'linear');

    img=uint16(interpolatedGrid/255 * (2^16-1));

    imwrite(img, strcat(outputDir, sprintf('%04d',w), '.png'));
end
end %end function
```